

Report No. FHWA-KS-04-1
FINAL REPORT

PERFORMANCE INVESTIGATION OF A FIBER REINFORCED COMPOSITE HONEYCOMB DECK FOR BRIDGE APPLICATIONS

Ondřej Kalný, M.S.C.E.
Robert J. Peterman, Ph.D., P.E.
Kansas State University



FEBRUARY 2005

KANSAS DEPARTMENT OF TRANSPORTATION

**Division of Operations
Bureau of Materials and Research**

1 Report No. FHWA-KS-04-1	2 Government Accession No.	3 Recipient Catalog No.	
4 Title and Subtitle PERFORMANCE INVESTIGATION OF A FIBER REINFORCED COMPOSITE HONEYCOMB DECK FOR BRIDGE APPLICATIONS		5 Report Date February 2005	6 Performing Organization Code
		8 Performing Organization Report No.	
7 Author(s) Ondřej Kalný, M.S.C.E., and Robert J. Peterman, Ph.D., P.E.		10 Work Unit No. (TRAIS)	
9 Performing Organization Name and Address Kansas State University Dept of Civil Engineering; 2118 Fiedler Hall Manhattan, Kansas 66502		11 Contract or Grant No. C1274	
		13 Type of Report and Period Covered Final Report April 2001 – January 2004	
12 Sponsoring Agency Name and Address Kansas Department of Transportation Bureau of Materials and Research 700 SW Harrison Street Topeka, Kansas 66603-3754		14 Sponsoring Agency Code RE-0292-01	
		15 Supplementary Notes For more information write to address in block 9.	
16 Abstract This report focuses mainly on the evaluation of stiffness and ultimate load-carrying capacity of Glass Fiber Reinforced Polymer (GFRP) honeycomb sandwich panels, with a sinusoidal core, used in bridge applications. Evaluation of fatigue performance is also included. Sixteen full scale panels with cross-section depths ranging from 5 in (125 mm) to 31.5 in (800 mm), instrumented with electrical resistance strain gages, displacement transducers, acoustic emission sensors and optical fibers for strain measurement, have been tested. A complete summary of experimental results is provided for each test, typically in the form of graphs of load vs. deflection and load vs. strain for all measured channels and photographs of failure modes. Coupon tests and shear tests on double lap specimens provided information about constituent material properties. The effect of width-to-depth ratio on unit stiffness was shown to be insignificant for panels with a constant depth of 6 in (150 mm) and width-to-depth ratios between one and five. A simple analytical formula for bending and shear stiffness, based on the material properties and geometry of a transformed section, was found to predict deflections within 20% accuracy. Although some factors influencing the ultimate load carrying capacity were clearly identified in this study, a reliable analytical prediction of the ultimate flexural capacity was not attained. This is due to the fact that failures occur in the bond lines between the outer faces and core, and that significant geometric variations along these bond lines can exist due to the wet layup process—even for theoretically identical specimens. Therefore, the use of wraps or internal ties (seven tested specimens had external wraps) is recommended. This serves to strengthen the relatively weak core-face interface and, as the research suggests, it could bring more consistency in determining the ultimate load-carrying capacity by shifting the ultimate failure from the resin bond material to the glass fibers. A preliminary proposal for design procedure of such wraps is presented. Finally, several 3D Finite Element models were developed and analyzed in order to better understand the behavior of these complex structural systems.			
17 Key Words FRP, GFRP, FRPH, bridge deck, honeycomb sandwich panel, wrap, composites, experimental testing, finite element modeling, deflection control, shear failure, bond failure, shear-friction		18 Distribution Statement No restrictions. This document is available to the public through the National Technical Information Service, Springfield, Virginia 22161	
19 Security Classification (of this report) Unclassified	20 Security Classification (of this page) Unclassified	21 No. of pages 118	22 Price

PERFORMANCE INVESTIGATION OF A FIBER REINFORCED COMPOSITE HONEYCOMB DECK FOR BRIDGE APPLICATIONS

Final Report

Prepared by

Ondřej Kalný, M.S.C.E.
Kansas State University

And

Robert J. Peterman, Ph.D., P.E.
Kansas State University

A Report on Research Sponsored By

THE KANSAS DEPARTMENT OF TRANSPORTATION
TOPEKA, KANSAS

KANSAS STATE UNIVERSITY
MANHATTAN, KANSAS

February 2005

© Copyright 2005, **Kansas Department of Transportation**

NOTICE

The authors and the state of Kansas do not endorse products or manufacturers. Trade and manufacturers names appear herein solely because they are considered essential to the object of this report.

This information is available in alternative accessible formats. To obtain an alternative format, contact the Office of Transportation Information, Kansas Department of Transportation, 700 SW Harrison Street, Topeka, Kansas 66603-3754 or phone (785) 296-3585 (Voice) (TDD).

DISCLAIMER

The contents of this report reflect the views of the authors who are responsible for the facts and accuracy of the data presented herein. The contents do not necessarily reflect the views or the policies of the state of Kansas. This report does not constitute a standard, specification or regulation.

ABSTRACT

This report focuses mainly on the evaluation of stiffness and ultimate load-carrying capacity of Glass Fiber Reinforced Polymer (GFRP) honeycomb sandwich panels, with a sinusoidal core, used in bridge applications. Evaluation of fatigue performance is also included. Sixteen full scale panels with cross-section depths ranging from 5-in (125 mm) to 31.5-in (800 mm), instrumented with electrical resistance strain gages, displacement transducers, acoustic emission sensors and optical fibers for strain measurement, have been tested. A complete summary of experimental results is provided for each test, typically in the form of graphs of load vs. deflection and load vs. strain for all measured channels and photographs of failure modes. Coupon tests and shear tests on double lap specimens provided information about constituent material properties. The effect of width-to-depth ratio on unit stiffness was shown to be insignificant for panels with a constant depth of 6-in (150 mm) and width-to-depth ratios between one and five. A simple analytical formula for bending and shear stiffness, based on the material properties and geometry of a transformed section, was found to predict deflections within 20% accuracy. Although some factors influencing the ultimate load carrying capacity were clearly identified in this study, a reliable analytical prediction of the ultimate flexural capacity was not attained. This is due to the fact that failures occur in the bond lines between the outer faces and core, and significant geometric variations along these bond lines can exist due to the wet lay up process—even for theoretically identical specimens. Therefore, the use of wraps or internal ties (seven tested specimens had external wraps) is recommended. This serves to strengthen the relatively weak core-face interface and, as the research suggests, it could bring more consistency in determining the ultimate load-carrying capacity by shifting the ultimate failure from the resin bond material

to the glass fibers. A preliminary proposal for design procedure of such wraps is presented. Finally, several 3D Finite Element models were developed and analyzed in order to better understand the behavior of these complex structural systems.

ACKNOWLEDGEMENTS

The authors would like to thank to the Federal Highway Administration (FHWA) and the Kansas Department of Transportation (KDOT) for funding the project. The authors would also like to acknowledge the following individuals for their contributions that enabled the completion of the research project and report:

Dave Meggers, of Kansas Department of Transportation, whose help with majority of the test setups is greatly appreciated. Dr. Jerry Plunkett and Russ Ricker, of Kansas Structural Composites, Inc., they supplied specimens for the testing, their transportation, and provided information about composite system being evaluated. Dr. Steve Cai for his involvement during the early stages of the project. Dr. Guillermo Ramirez conducted acoustic emission monitoring and provided several figures used in this report. In addition, Dr. Youchi Wang provided suggestions for finite element modeling and contributed with her expertise in composite materials, and Paul Lewis assisted with fatigue testing portion of this project.

TABLE OF CONTENTS

1	INTRODUCTION AND LITERATURE REVIEW.....	1
1.1	Introduction.....	1
1.2	Previous Research on Honeycomb Bridge Decks in Kansas.....	3
1.2.1	Report 1 (KSU): Two Years of Monitoring the First All Fiberglass Public Bridge [Walker and Held 1998].....	4
1.2.2	Report 2 (KSU): FRP Bridge Deck Design [Spears 2001].....	4
1.2.3	Report 3 (KU): Field Instrumentation and Monitoring of KDOT Fiber Composite Bridge for Long-Term Behavior Assessment [Adams et al. 2000].....	7
1.2.4	Report 4: Construction of a Composite Fiber-Reinforced Bridge in the State of Kansas [Hassan 2000].....	7
1.2.5	Report 5 (MU): Lateral Distribution in Kansas DOT Steel Bridge With FRP Deck [Schreiner 2000].....	8
1.3	Other Research.....	8
1.3.1	Hayes.....	8
1.3.2	Plunkett.....	9
1.3.3	Davalos et al.....	10
2	MATERIALS, SPECIMENS DESIGNATION AND EXPERIMENTAL PROCEDURES.....	11
2.1	Manufacture of Panels.....	11
2.2	Specimens Designation.....	14
2.3	Flexural Test Procedure.....	16
2.3.1	Use of Optical Fiber Strain Sensor System.....	18
2.4	Constituent Material Properties.....	18
2.4.1	Coupon Test Series #1 Results.....	20
2.4.2	Coupon Test Series #2 Results.....	21
2.4.3	Weight.....	22
3	EXPERIMENTAL RESULTS.....	23
3.1	Series A.....	23
3.2	Series A Repaired.....	27
3.2.1	A18 Repaired.....	28
3.2.2	A24 Repaired.....	30
3.2.3	A30 Repaired.....	32
3.2.4	A6 Repaired.....	33
3.3	32-ft-long Beams.....	34
3.3.1	Damaged Beam.....	35
3.3.2	Repair Procedure.....	35
3.3.3	32-ft-long Repaired Beam.....	37

3.3.4	Data Reduction Procedure	38
3.3.5	Comparison of Test Results from 32-ft-long Specimens.....	39
3.4	Panels Manufactured with Internal Steel Reinforcement.....	42
3.5	Double-Shear Specimens	42
3.5.1	Results from Tests of Unconfined Unwrapped Double-Shear Specimens (A1, A2, and A3).....	46
3.5.2	Results from Tests of Unconfined Wrapped Double-Shear Specimens (C1, C2, and C3)	50
3.5.3	Results from Tests of Confined Unwrapped Double-Shear Specimens (A4, A5, and A6).....	51
3.5.4	Summary of Test Results for Double-Shear Specimens.....	54
3.6	Fatigue.....	56
3.6.1	Fatigue Specimen 1	57
3.6.2	Fatigue Specimen 3.....	61
3.7	Summary	64
4	ANALYTICAL CALCULATION AND MODELS.....	65
4.1	Prediction of Shear and Flexural Stiffness from Material Properties	65
4.1.1	Sample Calculation of EI and GA (for Specimen A24 Repaired)	67
4.1.2	Sectional Properties and Stiffness for All Tested Specimens.....	69
4.1.3	Comparison of Theoretical and Experimental Deflections.....	69
4.1.4	Alternate Approach to Determine Flexural and Shear Panel Stiffness.....	70
4.2	Search for Failure Criterion.....	75
4.3	External Wrap and Shear Friction.....	80
4.3.1	Preliminary Recommendations for Wrap Design.....	82
4.4	FE Modeling.....	87
4.4.1	Meshing.....	87
4.4.2	Elements.....	90
4.4.3	Model 1: A6 (Overall Response)	91
4.4.4	Model 2: 32-ft-long Repaired Beam (Reduction of Stresses due to the External Wrap Layer).....	91
4.4.5	Model 3: A18 (Determination of Nodal Forces Acting Along Core-Face Interface)	94
5	CONCLUSIONS	99
6	SUGGESTIONS FOR FUTURE RESEARCH.....	102

APPENDICES AVAILABLE ON CD

- Appendix A: Project History
- Appendix B: Detailed Test Results
- Appendix C: Graphs Showing Results of FE Modeling of "Determination of Nodal Forces Acting Along the Core-Face Interface"

LIST OF FIGURES

Fig. 2.1: Sandwich Panel Geometry and Wrap Modification.....	12
Fig. 2.2: Face Lay-up Schedule (for 0.5 in Thick Face).....	13
Fig. 2.3: Load Profile for Acoustic Emission Monitoring (Graph Provided by G. Ramirez, University of Kansas).....	17
Fig. 2.4: Coupons Tested.....	20
Fig 3.1: Stiffness Comparison of Specimens Tested in <i>Series A</i>	25
Fig 3.2: Comparison of Ultimate Load per Unit Width for Specimens of <i>Series A</i>	25
Fig. 3.3: Schematic Drawing Showing the Re-bonding Layers and Wraps for the Repaired Specimens of <i>Series A</i>	28
Fig. 3.4: Development of Tension in the Wrap for A24 Repaired Specimen.....	31
Fig. 3.5: Total Load vs. Deflection (Comparison of Damaged, Repaired and Clarkson 32-ft-long Beams).....	40
Fig. 3.6: AE Results for Damaged Beam - Amplitude vs. Time (Graph Provided by G. Ramirez, University of Kansas).....	40
Fig. 3.7: AE Results for Repaired Beam - Amplitude vs. Time (Graph Provided by G. Ramirez, University of Kansas).....	41
Fig. 3.8: Double Shear Specimen.....	43
Fig. 3.9: Double Shear Specimen - Test Setup For "Confined Test" (2 in Thick Steel Plates Would Be Placed Along the External Faces to Ensure Proper Transfer of Lateral Force to the Load Cell).....	45
Fig. 3.10: Splitting of the Double-Shear Specimen.....	46
Fig. 3.11: Lateral Constraint for Double-Shear Specimen A3.....	47
Fig. 3.12: C-Clamps on Re-Instrumented Double-Shear Specimen A1.....	48
Fig. 3.13: Impact of Lateral Constraint on Double-Shear Specimens.....	49
Fig. 3.14: Lateral Restraint of Double-Shear Specimens by a Steel Frame.....	50
Fig. 3.15: Overall View of Confined Double-Shear Specimen, Steel Plates and Confining Steel Frame.....	52
Fig. 3.16: Detail of the Spreader Beam, Steel Plates and Top Portion of Confined Double-Shear Specimen.....	53
Fig. 3.17: Load Cell to Measure Lateral Force Developed by Confined Double-Shear Specimen	53
Fig. 3.18: Detail of the Bottom Portion of Confined Double-Shear Specimen, Steel Plates are Supported on Wooden Blocks (Photo).....	54
Fig. 3.19: Number of Days Between Beginning of the Test and Each Static Reading vs. Number of Accumulated Cycles (Fatigue Specimen 1).....	59
Fig. 3.20: Initial (Creep) Deflection on the Beam Prior to Each Static Test vs. No of Applied Cycles (Fatigue Specimen 1).....	59
Fig. 3.21: Load vs. Deflection for All Static Loadings (Fatigue Specimen 1).....	60
Fig. 3.22: Load vs. Strain for All Static Loadings (Fatigue Specimen 1).....	60
Fig. 3.23: Number of Days Between Beginning of the Test and Each Static Reading vs. Number of Accumulated Cycles (Fatigue Specimen 3).....	62
Fig. 3.24: Initial (Creep) Deflection on the Beam Prior to Each Static Test vs. No of Applied Cycles (Fatigue Specimen 3).....	62
Fig. 3.25: Load vs. Deflection for All Static Loadings (Fatigue Specimen 3).....	63

Fig. 3.26: Load vs. Strain for All Static Loadings (Fatigue Specimen 3).....	63
Fig 4.1: Sketch of Cross-Section of Specimen A24 Repaired.....	68
Fig 4.2: Comparison of Theoretical and Experimental Deflections	72
Fig 4.3: 3-point Bending Test.....	72
Fig 4.4: 4-point Bending Test.....	73
Fig 4.5: Photographs of Horizontal Shear Failure for Different Specimens.....	76
Fig 4.6: Ultimate Shear Flow for All Tested Flexural Specimens.....	78
Fig 4.7: Photos Showing Deformations in the Face Laminate of a FRPH panel.....	81
Fig 4.8: Drawing Illustrating Wrap Design (I.)	85
Fig 4.9: Drawing Illustrating Wrap Design (II.).....	86
Fig 4.10: Wrap Delamination—Stress Concentration Point.....	87
Fig 4.11: Typical Input File for MeshIt	89
Fig 4.12: FRPH Panel Mesh in ANSYS Generated by MeshIt	90
Fig 4.13: Deflection of A6 Panel Under Load in 3-pt Bending.....	91
Fig 4.14: Layer of Resin Elements in ANSYS Model.....	93
Fig 4.15: Reduction of Stresses in the Resin Interface due to the Wrap	93
Fig 4.16: Drawing Illustrating How Nodal Forces were Extracted	96

LIST OF TABLES

Table 2.1: Properties of Constituent Fiberglass Mats	12
Table 2.2: Properties of Tested Flexural Specimens	16
Table 2.3: Results of Coupon Tests from Series #1.....	21
Table 2.4: Results of Coupon Tests from Series #2.....	22
Table 2.5: Weights of Different Laminates in the Panel (Created with Regard to <i>Series A</i>)	22
Table 3.1: <i>Series A</i> - Dimensions and Description of Geometry.....	24
Table 3.2: <i>Series A</i> - Ultimate Load, Deflection, and Strain Data.....	24
Table 3.3: <i>Series A</i> - Comparison of Total Weight for the Original and Repaired Specimens	28
Table 3.4: Series A Repaired—Ultimate Load, Deflection and Strain Data	34
Table 3.5: Double-Shear Test—Results	55
Table 3.6: Summary of Test Results for All Flexural Test Specimens	64
Table 4.1: Calculation of Sectional Properties for Specimen A24 Repaired (Refer to Figure 4.1)	69
Table 4.2: Summary of Sectional Properties for All Tested Specimens.....	70
Table 4.3: Comparison of Theoretical and Experimental EI and GA for Series A	74
Table 4.4: Comparison of Theoretical and Experimental EI and GA for Fatigue Baseline Specimen	75
Table 4.5: Sum of Nodal Forces Along Flats, Flutes, and Core	97

ACRONYMS AND ABBREVIATIONS

ACI American Concrete Institute

AE Acoustic Emission

DA, DAQ Data Acquisition

FE Finite Elements

FRP Fiber Reinforced Polymer

FRPH Fiber Reinforced Polymer Honeycomb

KDOT Kansas Department of Transportation

KSU Kansas State University

KU University of Kansas

KSCI Kansas Structural Composites, Inc.

LVDT Linear Variable Differential Transducer

GLOSSARY OF TERMS

Core. Core of the sandwich panel. Corrugated core with alternating flat and sinusoidal plates was used for panels evaluated in the scope of this report.

Face. Top or bottom surface (skin) of the sandwich panel.

Flat. Flat plate of the core of sandwich panel.

Flute. Sinusoidal plate of the core of sandwich panel.

Sandwich Panel. Structural member made up of two stiff, strong faces (skins) separated by a light-weight core. The separation of the faces by a light-weight core significantly increases the moment of inertia with only a small increase in weight—resulting in a very efficient structure.

Web. A thin vertical plate connecting the upper and lower flanges the idealized I-beam that is used to represent the sandwich panel cross-section for simplified calculations.

Chapter 1

Introduction and Literature Review

1.1 Introduction

According to the National Bridge Inventory Study Foundation (NBISF) survey completed in 2000, about 27% of the bridges in the United States are classified as structurally deficient or functionally obsolete. Moreover, the NBISF recommends that nearly one in every four bridges should be replaced due to substandard load carrying capacity or substandard bridge roadway geometry [NBISF 2002].

Bridge owners are continually investigating methods to effectively retrofit existing bridges, or to economically replace them with new ones. Modern composite materials for structural applications, formerly only in the domain of aerospace engineering, are increasingly making their way into the civil engineering sphere. In addition to retrofitting current concrete and steel structures, especially with Carbon Fiber Reinforced Polymer (CFRP) plates, a great deal of work is being conducted to develop versatile, fully-composite structural bridge systems. Although composites have become financially competitive with more traditional materials, cost is still the primary factor limiting their widespread use. Therefore, cheaper glass fibers and polyester or vinyl ester resins are favored for all-composite structural systems, and a number of pedestrian and highway bridges utilizing these materials are currently in service (refer to [Bakis et al. 2002] and Sec. 1.3.1).

Several different approaches to creating stand-alone structural systems are currently being employed. These differ from each other in the manufacturing processes (including wet hand lay-up, pultrusion, and resin transfer molding), component section geometry (I-Beams,

tubular members, sandwich panels with various core materials) and how the systems are assembled together for the desired structural application [Szak et al. 1999, Bank and Yin 1999, Lopez-Anido and Xu 2002, Hayes 1998, Bakis et al. 2002].

This report presents findings from both experimental and analytical evaluations of a Fiber Reinforced Polymer (FRP) structural honeycomb bridge system. The system was developed by Kansas Structural Composites, Inc. (KSCI), which has successfully installed fully-composite bridges in several states including Kansas, Missouri, and West Virginia. The bridge members are fabricated manually using a wet lay-up process—the design utilizes sandwich panel with a light-weight honeycomb core. These panels have been used both as conventional decks (spanning transversely between concrete or steel girders) and as deckbeams (spanning longitudinally between abutments), refer to Section 1.2.

The main topics covered in this report include:

1. Investigation of width-to-depth ratio on unit stiffness.
2. Stiffness determination both experimentally and analytically.
3. Identification of failure criteria.
4. Contribution of external corner wraps to the increase of ultimate bearing capacity.
5. Evaluation of the size effect on ultimate capacity.
6. A preliminary proposal for the design of wrap.
7. Evaluation of fatigue performance.

Development of rigorous 3D Finite Element (FE) model and several analyses that were run are presented. Acoustic Emission (AE) monitoring was done by the University of Kansas (KU) and is briefly discussed in general without providing the details about procedures and results.

Since the work conducted was primarily experimental and helped to establish a database of test results that are of great importance for composite structures, the test data are presented in significant detail in Appendix B. These include drawings of test setups and instrumentation, graphs summarizing test results and photographs of failure modes. The database can serve not only to KSCI to extend their current database about properties of their products, but to other researchers as well [detailed data is available on CD by contacting Robert Peterman, Associate Professor, at bob@ksu.edu or (785) 532-7612]. This is due to the fact that the studied phenomena (e.g. the effects of wraps or ties) will have general applicability to other composite structural shapes¹ and are not limited to a specific product or a specific manufacturer. The typical failure mechanism of FRPH sandwich panels manufactured by KSCI is similar to that of delamination in 2D laminates—the system fails in resin before the ultimate capacity of fibers can be reached. The current composite industry widely uses two-dimensional laminates that are prone to the delamination failure. To overcome this frequent mode of failure, several types of 3D braiding machines have been proposed [Zhou 1999] to produce three-dimensional delamination-free braided composites. Reinforcing relatively weak core-face interface in KSCI's panels might prevent delamination by providing continuous fiber over the critical interface—this idea is similar to that behind 3D braided composites.

1.2 Previous Research on Honeycomb Bridge Decks in Kansas

Considerable research on the structural system evaluated in this report has been done previously at KSU. This work included the proof testing and monitoring of the No-Name Creek Bridge (see Section 1.3.2) as well as laboratory testing of panels with distinct characteristics, and was a part of broader activity by KDOT aimed at investigating the feasibility of FRPH bridge decks. During

¹ Bank and Yin [Bank and Yin 1999] studied failure of web-flange junction in pultruded I-beams. They concluded that placement of biaxial fabrics in the junction region can decrease the likelihood of web-flange separation failure mode.

and after the period of installation of three pioneering FRPH bridges in Kansas (bridge over No Name Creek West of Russell, Russell County, installed 1996; two bridges on Kansas State Highway 126 (K-126) West of Pittsburg, Crawford County, installed 1999), KDOT was endeavoring to develop a design manual for future FRPH bridges in Kansas. KDOT cooperated with several educational, industry, and state institutions, namely KSU, KU, University of Missouri (MU), KSCI who constructed all the deck samples, and the Federal Highway Administration (FHWA).

The only documentation about previous research for KDOT (other than that listed in Section 1.3) known to the author was compiled by Paul Spears, an undergraduate research assistant at KSU. This includes five separate reports which are described in more detail in the following paragraphs.

1.2.1 Report 1 (KSU): Two Years of Monitoring the First All Fiberglass Public Bridge [Walker and Held 1998]

By Dr. Hugh Walker, Professor and John J. Held, Research Engineer

This report describes proof testing of the No-Name Creek Bridge. The design of the bridge by Professor Walker was based on about 100 composite panels previously tested. Creep testing of the installed bridge did not indicate any significant changes and was overshadowed by weather-induced deformations (e.g. the panel bowed up when its upper face was heated up by sun). There was no significant change in stiffness and creep after 24 months from installation. Data after 24 months was not available at the time of this report.

1.2.2 Report 2 (KSU): FRP Bridge Deck Design [Spears 2001]

Compiled by Paul W. Spears, based on the work of Walker and Held

Since the public safety is the primary design principle, and since it was the first bridge of its kind, the bridge over the No-Name Creek was considerably over-designed. Therefore KDOT later concentrated their efforts and resources into research aimed at optimizing the design of FRP

bridge decks. Based on the premise that it is difficult to analytically predict how the bridge decks would perform, even though the composition of the panel is well known, it was decided to study the deck as a whole. Practically, this meant that entire deck panels were constructed with subtle changes so that the effect of the changes on the performance of entire structure could be analyzed. To isolate the variables, five sets of deck panels were tested. Each set consisted of panels with various core geometries and “one other distinct characteristic.” This arrangement served two purposes. First, the core geometries within the sets could be evaluated relative to the other cores in the set. Secondly, the “one other distinct characteristic” between the sets could be compared since the core geometries among the different sets were consistent.

The following sets were tested:

- **Set 000** - It was manufactured before the test program, included many variations (core depth, flat and flute thickness, face thickness) and was tested only to obtain some preliminary information.
- **Set 001** - Varying core geometry with essentially no faces (just a thin bonding layer).
- **Set 002** - Similar to Set 001, except that all specimens had top and bottom faces.
- **Set 003** – Re-used Set 001 specimens and 3/8-in thick faces were added.
- **Set 004** - Re-used Set 002 with the addition of a 1/2-in thick layer of polymer concrete overlay on the top face to study its contribution to stiffness.
- **Set 005** - Included samples with varying thicknesses of core laminate.

Several different tests were conducted on above described sets of samples or their constitutive materials. These test included:

- Coupon tests
- Punch and crush tests
- Three and four point bending tests

- Shear tests
- Fatigue tests (however in a very limited extent)

The following list summarizes the results and conclusions from Walker and Held:

- **Coupon tensile test** of both face and core laminate yielded great variation between test data that were marked as “impertinent or erroneous.”
- **Set 000** was used to calculate bending stiffness EI and shear stiffness GA from different spans of identical beams tested in 3-point bending employing Equation 1.1:

$$\delta_{total}(L/2) = \delta_{bending} + \delta_{shear} = \frac{PL^3}{48EI} + \frac{PL}{4GA} \quad (\text{Eqn. 1.1})$$

For EI, good correlation between theoretical² and experimental values was obtained. However, GA did not seemingly follow any pattern. Punch and crush tests revealed that thickness of the top face and presence of a polymer concrete overlay are the major factors enhancing punch and crush strengths. It was later learned by the authors from a conversation with Dr. Plunkett of KSCI that after removing the maximum sustainable load from the panel, the core recovered its original state without permanent damage.

- Comparison between **Sets 001 and 003** confirmed the theoretical expectations that the core primarily resisted shear deformation while the faces provided the main flexural resistance. An interesting observation was that the samples of Set 001 (without faces) had a similar stiffness for both longitudinal and lateral orientation of the core.
- Comparison between **Sets 002 and 004** indicated that the polymer concrete overlay served to increase EI, but not in a predictable magnitude. The change in GA with the addition of polymer concrete was also sporadic.

² Theoretical EI was based on average E from coupon tests after several external values were dropped out and I was based only on contribution of faces.

- Evaluation of the test results from samples in **Sets 001 to 004** suggested that a sinusoidal core with alternating flat and sinusoidal plates (currently used by KSCI in their manufacturing process) provides the best combination of shear and bending stiffness values.
- Finally, **Set 005** showed that GA increases for panels with thicker flats and flutes and for samples with cores made of tri-directional fiber mats³. However, KSCI currently uses Chop Strand Mats as the core material

1.2.3 Report 3 (KU): Field Instrumentation and Monitoring of KDOT Fiber Composite Bridge for Long-Term Behavior Assessment [Adams et al. 2000]
By Jeffrey S. Adams, Dr. Guillermo Ramirez, and Dr. JoAnn Browning

The first part of the report presents results of the literature search conducted to gather information about Non-Destructive Evaluation (NDE) and Structural Health Monitoring (SHM) techniques and typical sensors used to monitor civil structures. This will assist KDOT in selecting feasible method for long-term monitoring of FRPH bridges.

The second part describes FE modeling of the bridge in Crawford County, Kansas. The main model, developed to simulate the behavior of the bridge as a whole, consisted of steel wide flange sections, FRP saddle beams and a tributary portion of the FRP deck panel. A submodel was used to get more accurate results in the connection area between the steel girder, FRP saddle beam, and FRP deck panel. The model was evaluated for several loading cases, including static, thermal, and dynamic loads.

1.2.4 Report 4: Construction of a Composite Fiber-Reinforced Bridge in the State of Kansas [Hassan 2000]
By Damon Hassan, FHWA Engineer, Kansas Division

This report describes the replacement of substandard corrugated metal decking with an asphalt overlay by new FRPH decking on the bridge in Crawford County, Kansas.

³ Fibers are oriented in 3 principal directions, which results in increased panel shear stiffness—superior to shear stiffness for panels where uniaxial or Chop Strand Mats are used to laminate flats and flutes.

1.2.5 Report 5 (MU): Lateral Distribution in Kansas DOT Steel Bridge with FRP Deck [Schreiner 2000]

*By John Schreiner and Michael Barker, P.E., Dept. of Civil Engineering,
University of Missouri, Columbia*

This report compares the lateral distribution (lateral stiffness) of the original 14-girder Crawford County bridge with an asphalt deck to the lateral distribution of the same bridge after rehabilitation with FRPH decking. Field experimental testing indicated a similar distribution existed for both types of decking.

1.3 Other Research

1.3.1 Hayes

Hayes [Hayes 1998] presents an extensive literature review and summary of the current (year 1998) situation in all-composite structural systems. The summary, compiled from many resources, starts by reviewing the current state of U.S. infrastructure and provides estimates of how many insufficient bridges need to be replaced or rehabilitated on tight financial constraints. A comparison of the initial costs and maintenance costs, over the typical bridge life span, is made for bridges of conventional materials and FRP. As a result of this comparison, the growing interest in utilizing FRP composite materials is addressed. Next, advantages (high stiffness- and strength-to-weight ratios, fatigue resistance, corrosion resistance, light weight, suitability for prefabrication, life cycle cost-effectiveness) and drawbacks (higher initial cost, physical and chemical aging, low stiffness, connection design and complicated failure mechanisms, limited ductility prior to failure, creep performance) of FRP systems are discussed.

Different fiber (carbon, aramid, glass) and resin (polyester, vinyl ester, epoxy) systems, manufacturing processes and achievable member shapes are listed. A few milestone pedestrian bridges a total of over 60 currently in service in the U.S. are shortly introduced. These include:

LaSalle Street pedestrian walkway (1996, over Chicago River), Antioch composite bridge (1995, Antioch Golf Club, Illinois), two FRP pedestrian bridges in Golden Gate National Recreational Area in San Francisco (constructed by E.T Techtonics), pedestrian bridge in Daniel Boone National Forest (1996, Kentucky) and bridges on the campus of University of California (San Diego, group of Frieder Seible). Several traffic bridges, that are still mainly experimental or demonstrational and serve as test cases for design and long term performance evaluation are also introduced: Bonds Mill Lift bridge (Stroud, England), Laurel Lick bridge (Lewis county, West Virginia, 1997), Wickwire Run bridge (Taylor County, West Virginia, 1997), “INEEL” bridge (Idaho, 1995), “Tech 21 Bridge” (Ohio, 1997), Magazine Ditch bridge (Delaware, 1997). Further in the report, several major groups developing composite structures and their products are introduced. Shear deformation and typical failure criteria are summarized. Usual practices and several case studies for conducting fatigue and creep tests are compiled.

The Hayes’s report itself focuses on the experimental evaluation and analytical characterization of pultruded hybrid⁴ composite double-web I-Beams with sub-flanges that have been used in the rehabilitation of Tom’s Creek Bridge in Virginia.

1.3.2 Plunkett

Plunkett [Plunkett 1997] presented general design and marketing concepts for the bridge system that has been evaluated within the scope of this report. Moreover, detailed information about the manufacturing process is provided. A portion of the text is devoted to the proof testing and installation of the No-Name Creek FRP bridge in Russell County, Kansas, the very first bridge installed by KSCI in November 1996.

⁴ Both glass and carbon fibers were used.

1.3.3 Davalos et al.

Davalos et al. [Davalos et al. 2001] introduced an analytical formula to determine the longitudinal and transverse stiffness of FRP honeycomb sandwich panels with sinusoidal core geometry (the same system as evaluated in this report). This formula is derived purely mathematically from fundamental fiber and matrix properties and panel geometry. Using micromechanical principles, homogenization methods, and classical lamination theory, apparent beam stiffness was obtained. Results compared reasonably well to FE model and experimental data. The reader of this report is encouraged to also refer to numerous papers authored or co-authored by Davalos [Bakis et al. 2002, Davalos et al. 2001, Xu et al. 2001, Qiao et al. 2000, Davalos and Qiao 1999], because part of his work was based on the evaluation of the FRPH sandwich panel system manufactured by KSCI – the same system that is studied in this project.

Chapter 2

Materials, Specimens Designation and Experimental Procedures

2.1 Manufacture of Panels

All panels and beams tested in the experimental program were manufactured at the KSCI production facility in Russell, Kansas, using a wet hand lay-up process. The constituent materials were E-glass fiber in the form of mats (supplied by Brunswick Technologies Inc., Brunswick, Maine) and polyester or vinyl ester resin.

The sandwich panels (Figure 2.1) are composed of two outer faces (which primarily provide the flexural rigidity) and a core that is used to maintain the distance between the faces and to carry shear. The corrugated core is typically manufactured of Chop Strand Mat (ChopSM) and consists of alternating flat and sinusoidal plates (referred to as flats and flutes, respectively). Each plate is laminated separately. Flats and flutes are bonded together by placing a cured flat on top of a wet flute and allowing the assembly to cure. The whole core is then manufactured by sequentially bonding the flat-flute assemblages together using polyurethane adhesive.

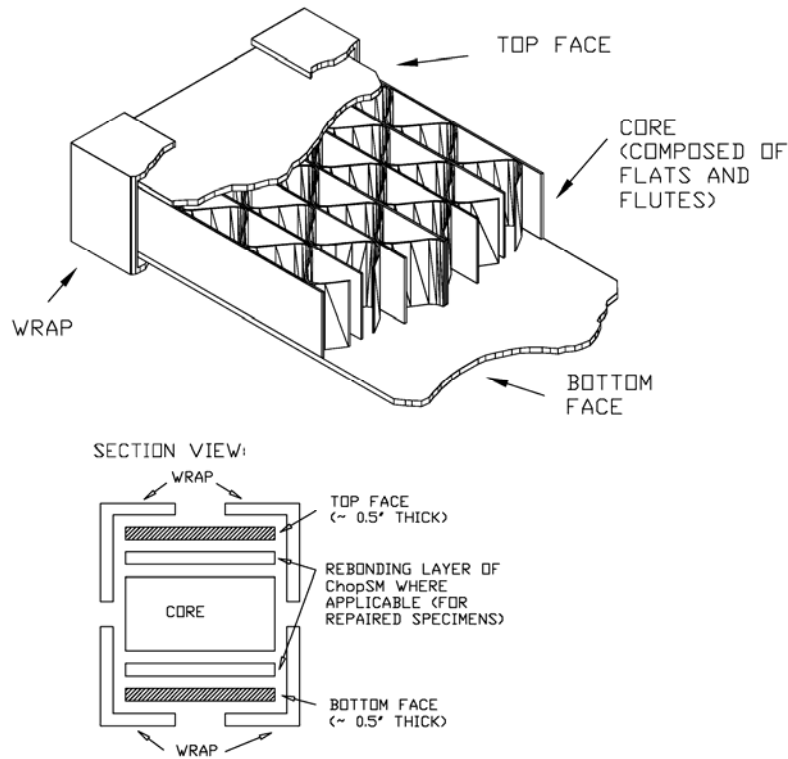


Figure 2.1: Sandwich Panel Geometry and Wrap Modification

E-glass fiber mats were used in four different kinds of fiber architecture as described below (A summary of the individual layer properties is provided in Table 2.1):

Table 2.1: Properties of Constituent Fiberglass Mats

Ply name	Constituent laminae	Nominal weight	Thickness
Bonding and wrap layer	ChopSM	3.0 oz/ft ² (915 g/m ²)	0.082 in (2.08 mm)
Core mat	ChopSM	4.5 oz/ft ² (1373 g/m ²)	0.090 in (2.29 mm)
CM3205	0°	16/9 oz/ft ² (543 g/m ²)	0.0245 in (0.622 mm)
	90°	16/9 oz/ft ² (543 g/m ²)	0.0245 in (0.622 mm)
	ContSM	0.5 oz/ft ² (153 g/m ²)	0.01 in (0.254 mm)
UM1810	0°	2.0 oz/ft ² (610 g/m ²)	0.025 in (0.635 mm)
	ContSM	1.0 oz/ft ² (305 g/m ²)	0.013 in (0.330 mm)

Based on measurements of various panels, following average values were determined:

- (1) Thickness of 3 layers of 3.0 oz ChopSM (re-bonding layer, wrap on *Series A Repaired*): 0.25 in
- (2) Thickness of 1 layer of 3.0 oz ChopSM (wrap for 32-ft-long Beams): 0.095 in
- (3) Thickness of 1 layer of 4.5 oz ChopSM (flats and flutes): 0.115 in
- (4) Thickness of top and bottom face: 0.5 in

- Chopped Strand Mat (ChopSM) consists of short fibers randomly oriented. ChopSM is used to fabricate the flats and flutes as well as between the core and face laminate to provide a uniform and resilient bond layer.
- Continuous Strand Mat (ContSM) consists of continuous randomly oriented fibers and is used to provide a backing for other layers.
- Bi-directional ($0^0/90^0$) stitched fabric with a balanced number of fibers running in orthogonal direction (designation CM3205).
- Unidirectional 0^0 layer of fibers (designation UM1810).

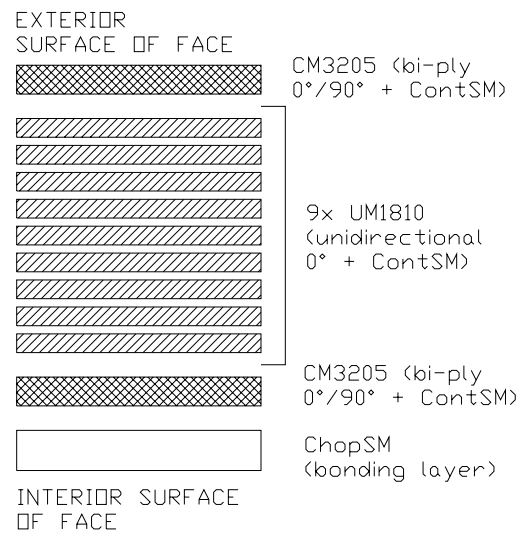


Figure 2.2: Face Lay-up Schedule (for 1/2-in Thick Face)

The top and bottom faces are fabricated by consecutively stacking resin-soaked plies (according to lay-up schedule shown in Figure 2.2) on top of each other. Then, the sandwich panel is constructed by placing the core sections on top of the face laminate while the resin is still wet. The core is then pressed into the face laminate using dead weight and is allowed to cure.

After curing, the other face laminate is applied to finish the sandwich panel. The sandwich core cell geometry, composed of flats and sinusoidal flutes (Figure 2.1) was used for all specimens evaluated in this study.

Some panels were repaired and tested again. Repair of panels was deemed plausible, since typical flexural failures occurred at the bond interface between the core and face, leaving the core and face laminates virtually untouched. During the repair procedure, each face was totally removed from the core and re-bonded back using an additional layer of 3-oz ChopSM. Then, external wraps were applied over the edges (Figure 2.1).

The typical surface treatment for bridge panels consists of a resin-based concrete mix (polymer concrete), which provides an acceptable wearing surface. This surface was not applied to the test specimens in this study, since it does not contribute to the structural properties used in design.

2.2 Specimens Designation

The deck specimens evaluated in this study had following designations:

- *Series A*, a total of five panels (designated *A6*, *A12*, *A18*, *A24* and *A30*; the number identifies specimen's nominal width in inches) were tested. The objective of this test series was to determine if there is an effect of the specimen's width-to-depth ratio on flexural properties (for panels of constant depth), in terms of both stiffness and ultimate load-carrying capacity, per unit width.
- Four of the specimens from *Series A* (*A6*, *A18*, *A24* and *A30*) were repaired after they were loaded to failure. These four specimens incorporated the repair and wrap improvements explained in Section 2.1. It is worth noting that the repair procedure resulted in a significant increase in both the stiffness and weight, primarily due to the application of the three re-bonding ChopSM layers. These repaired specimens were designated as *Series A Repaired*.

- Three *32-ft-long* specimens were also analyzed in this study. These were denoted as *32-ft Clarkson* (tested at Clarkson University under direction of Dr. Maria del Mar Lopez; data about this beam used in this report were provided by Dr. Jerry Plunkett (KSCI)), *32-ft Damaged* and *32-ft Repaired*. All three specimens had a similar overall geometry. The difference between them was that the *32-ft Damaged* specimen had a pre-existing partial core-face delamination, while the *32-ft Repaired* specimen was repaired (using the scheme described in Section 2.1) after the *32-ft Damaged* specimen had been tested to failure. The *32-ft Clarkson* specimen was undamaged prior to being loaded to failure.
- Two *Steel Reinforced* specimens (*Steel 2 Rebars* and *Steel 4 Rebars*) implemented steel reinforcement within the faces as well as external wrap.
- *Fatigue Series* consisted of four identical specimens that were cut out of one larger panel. *Fatigue Baseline* was statically tested to failure to determine the base stiffness and strength before the two other specimens (*Fatigue Specimen 1*, *Fatigue Specimen 3*) were tested in fatigue under different span to deflection ratios. *Fatigue Specimen 2* had not been tested at the time of this report.

A summary of the tested flexural specimens, including calculated section properties and loading geometry is provided in Table 2.2. In addition to the flexural test, tests were also conducted on *coupons* to determine the constituent material properties and on *Double Shear* specimens to assess the bond strength between the core and faces.

Table 2.2: Properties of Tested Flexural Specimens

Specimen	I_{trans} [in ⁴]	A_{core} [in ²]	Wrap	h [in]	w [in]	l [ft-in]	Test Setup	Cells Per Width	Resin
A6	132.2	3.43	—	5.9	7.1	8' – 4"	3-pt	3	polyester
A12	257.4	6.79	—	5.9	13.2	8' – 4"	3-pt	6	polyester
A18	388.5	10.08	—	5.9	19.8	8' – 4"	3-pt	9	polyester
A24	490.3	13.53	—	5.9	25.5	8' – 4"	3-pt	12	polyester
A30	666.3	15.20	—	5.9	32.1	8' – 4"	3-pt	15	polyester
A6 Repaired	233.5	6.47	YES	6.9	7.6	8' – 4"	3-pt	3	polyester
A18 Repaired	604.4	12.67	YES	6.9	20.3	8' – 4"	3-pt	9	polyester
A24 Repaired	746.4	16.55	YES	6.9	26.0	8' – 4"	3-pt	12	polyester
A30 Repaired	973.9	18.10	YES	6.9	32.6	8' – 4"	3-pt	15	polyester
Fatigue Baseline	699.5	12.60	—	8.0	19.5	14' – 5"	4-pt	8	polyester
Fatigue Specimen 1	699.5	12.60	—	8.0	19.5	14' – 5"	4-pt	8	polyester
Fatigue Specimen 3	699.5	12.60	—	8.0	20.0	14' – 5"	4-pt	8	polyester
32ft Damaged	10,117.9	42.09	—	31.5	12.0	32'	4-pt	6	vinyl ester
32ft Clarkson	10,389.8	45.60	—	31.5	12.0	32'	4-pt	6	vinyl ester
32ft Repaired	11,617.0	45.60	YES	31.5	12.0	32'	4-pt	6	vinyl ester
Steel 2 Rebars	206.0	7.78	YES	5.0	12.0	10'	3-pt	6	polyester
Steel 4 Rebars	238.1	7.78	YES	5.0	12.0	10'	3-pt	6	polyester

I_{trans} : moment of inertia of section transformed into the core (ChopSM) material

A_{core} : area of sandwich core

Wrap: YES indicates that there was wrap on the panel, — indicates no wrap

h: total height of the cross-section

w: width of the cross-section

l: length of the panel

Test Setup: 3-pt means three-point bending, 4-pt means four-point bending

2.3 Flexural Test Procedure

All panel specimens were tested in either three-point or four-point bending as listed in Table 2.2.

At the beginning of the test program, tests were conducted using hydraulic actuators in “load control.” Load-controlled tests resulted in sudden failures upon reaching the ultimate flexural capacity and it was therefore decided to switch to deflection (stroke) control for subsequent tests (refer to Appendix A). The major benefit of deflection-controlled tests was the opportunity to track progressive failures; this was found very useful in confirming the internal load paths and failure mechanism. Tests were conducted in three different loading frames (including the 500 kip (224 kN) capacity Havens Steel Self-reacting outdoor frame) in order to accommodate

requirements for failure load levels for specimens of different sizes. A data acquisition system was used to acquire deflection data from LVDTs, strain data from electrical resistance strain gages and applied load data from load cells. Most of the test specimens were instrumented with multiple strain gages (several panels had over 20 strain gages each) to obtain strain data at locations where phenomena related to the ultimate failure was likely to occur⁵. Since the phenomena usually occurred only in one location, useful discussion about the failure can be made primarily for gages mounted in that location. All other gages provided data that was not directly related to the studied failure phenomena and have been omitted from subsequent discussions. These gages, however, were applied in case failure initiated in their vicinity.

Acoustic Emission (AE) data were recorded for the majority of the tests. For the purpose of AE, a special loading profile (consisting of load holds, load drops and load increases, refer to Fig. 2.3) was designed to assess AE signature characteristics such as Felicity Ratio.

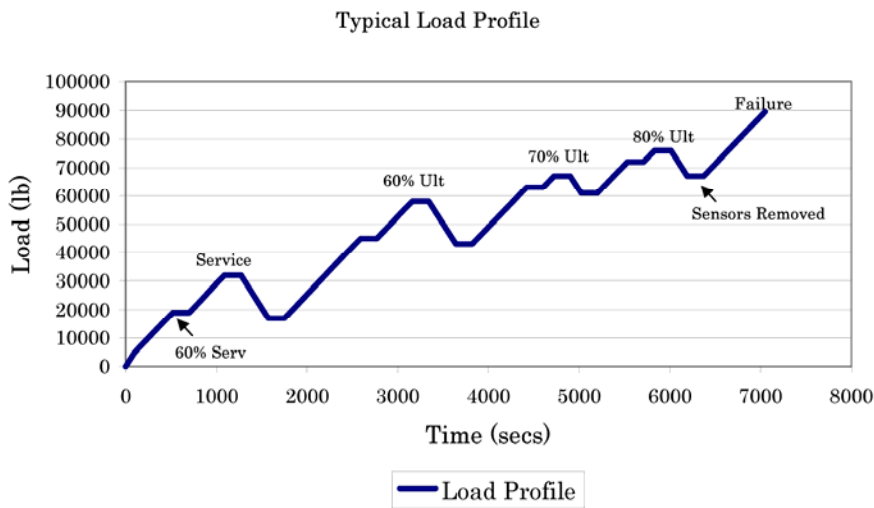


Figure 2.3: Load Profile for Acoustic Emission Monitoring (Graph Provided by G. Ramirez, University of Kansas)

⁵ For wrapped specimens, wrap delamination usually occurred only along one side of the panel, and was further limited to the portion of the panel from support to the midspan. The delamination could possibly occur in four locations, but actually occurred only in one location that could not be predicted beforehand. Therefore, all four locations were instrumented with strain gages.

During the test several nylon straps were loosely placed around the specimens to prevent fragments of the failed specimens from becoming projectiles and to ensure the safety of all test observers.

2.3.1 Use of Optical Fiber Strain Sensor System

Developed by British engineers [Smart Fibers Ltd: OFSSS], optical fibers are a very perspective tool of strain analysis. This is true especially for composite materials, where fibers can be embedded directly into the composite body. Strain is correlated to the wavelength of the light beam traveling through the glass fiber. The wavelength change is proportional to the strain and is caused by a sensor placed within the fiber at desired location. The portion of the glass fiber with sensor is glued to the surface of interest.

For the *32-ft Damaged* specimen, optical fibers were also used for strain measurements. These optical fibers were embedded “inside the beam” during the fabrication process. Data acquisition from these fibers was carried out by a representative of *Smart Fibers, Ltd.* Due to certain hardware problems, however, only a fraction of the strain data was recorded. Comparison with strain values obtained from the *32-ft Repaired* beam test, where electrical resistance strain gages were used for strain measurements, shows reasonably close agreement.

2.4 Constituent Material Properties

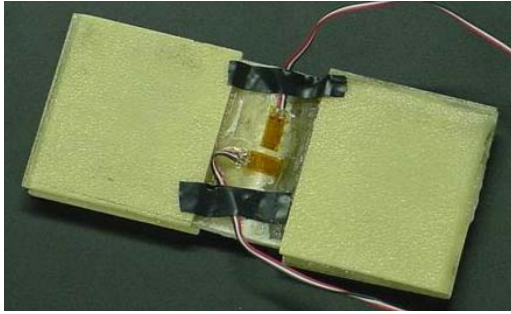
The material properties of the core and face laminates have been determined both analytically and experimentally.

The analytical approach proposed by Davalos et al. [Davalos et al. 2001] uses mechanical properties of the fiber and resin, fiber volume fraction, and fiber orientation (random or unidirectional) as fundamental inputs for determination of the properties of a single lamina using a micro-mechanical approach. Then, based on the stacking sequence of the laminate, the

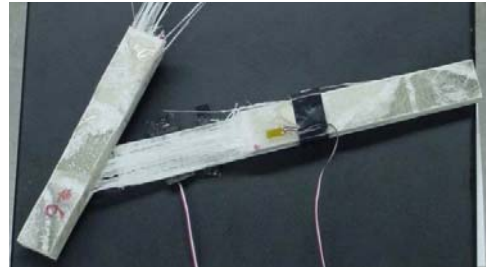
laminates properties can be calculated using classical lamination theory. Continuing in this scheme, the apparent stiffness of the core can be calculated using homogenization and energy methods and finally, the apparent sandwich beam stiffness can be obtained. The analytical work conducted by Davalos et al. was based on sandwich panels that were supplied by KSCI, the same manufacturer that supplied all of the specimens tested at KSU. Since KSCI has not changed their fabrication process during the time of the previously mentioned research programs, the expressions for material properties derived by Davalos et al. were also valid for KSU test specimens. Namely, the stiffness properties (Young's modulus, shear modulus and Poisson's ratio) of the core and face laminates from the analytical model can be directly compared to coupon test results conducted at KSU.

Coupon tests on the actual manufactured core and face laminates (Figure 2.4) provided material properties at the highest point of the fabrication process. This is believed to represent the actual values more closely, because manual fabrication may result in imperfections that can influence stiffness properties.

A comparison was made between the coupon test results and the theoretical properties predicted by Davalos et al. [Davalos et al. 2001]. The calculated core laminate stiffness is higher than the experimental one; the longitudinal Young's modulus for the face is approximately the same, while the theoretical face transverse modulus is lower. In all cases, the calculated properties were within 30% of those determined from actual coupon tests.



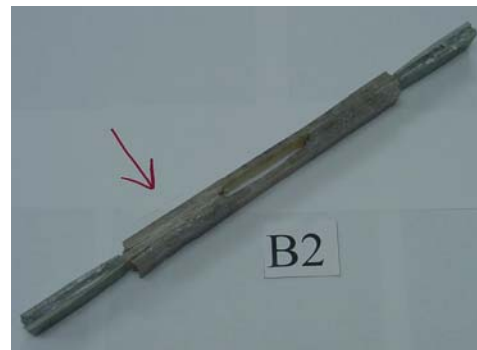
(a) Compression Coupon of Core Laminate



(b) Tension Coupon of Face Laminate



(c) Tension Coupon of Core Laminate



(d) Double Lap Secondarily Bonded Shear Coupon

Figure 2.4: Coupons Tested

2.4.1 Coupon Test Series #1 Results

Results from coupon tests from series #1 are summarized in Table 2.3. A set of 10 coupons (three compression coupons of the core laminate, four tension coupons of the core laminate and three tension coupons of the face laminate) was tested in compression and tension. Table 2.3 lists average properties based on tension and compression tests for the core laminate and on tension test only for the face laminate⁶. The coupons were extracted from specimen A12 after it had been tested to failure.

⁶ For core ChopSM, the properties in tension and compression were almost identical.

Table 2.3: Results of Coupon Tests from Series #1

	Core mat	Face laminate 0°	Face laminate 90°
E	1.176 Msi (8.11 GPa)	2.796 Msi (19.28 GPa)	2.180 Msi (15.03 GPa)
ν_{12}	0.312	0.278	0.196
G	0.448 Msi (3.09 GPa)	—	—
σ_{ult}	16.3 ksi (112 MPa)	27.3 ksi (202 MPa)	16.4 ksi (113 MPa)
ϵ_{ult}	14,860 $\mu\epsilon$	9,700 $\mu\epsilon$	11,000 $\mu\epsilon$

Core mat (ChopSM) can be considered as isotropic material due to the random orientation of short fibers, then: $G = E / (2(1+\nu))$

2.4.2 Coupon Test Series #2 Results

In the coupon test series #2, nine coupons were tested. All of them were manufactured to determine the tension and shear properties of the wrap laminate (composed of three layers of 3.0 ChopSM), which was used during the repair and strengthening of several specimens. Three coupons designated *A1* to *A3* were double lap simultaneously cured shear coupons, three coupons *B1* to *B3* were double lap secondarily bonded shear coupons and finally *C1* to *C3* were simple tension coupons (Refer to Figure 2.4). All three “A” coupons failed by tension of the single layer in the contracted region resulting from manufacturing process. Therefore, they would provide only a lower bound value of shear strength, and not the shear strength itself. Coupons “B” all failed in shear at level that is only 37% higher than the lower limit of group “A”.

Table 2.4: Results of Coupon Tests from Series #2

	Shear coupons cocured	Shear coupons secondarily bonded
τ_{ult}	414.6 psi (2.86 MPa) (LOWER BOUND)	571.4 psi (3.94 MPa)

Tension coupons	
E	1.150 Msi (7.93 GPa)
σ_{ult}	14.8 ksi (102 MPa)
ϵ_{ult}	14,313 $\mu\epsilon$

2.4.3 Weight

In order to estimate the weight of the previously tested panels, and to characterize the component unit weights, flats, flutes, and faces of the failed *A12* panel were weighted and Table 2.5 was created. The table was created with regard to *Series A*, but can be used to estimate the weight of any deck specimens prepared using the same lay-up process.

**Table 2.5: Weights of Different Laminates in the Panel
(Created with Regard to Series A)**

	Area or amount	Weight [lb]
Flute	one flute (length: 104 in, height: 5 in)	5.096
Flat	one flate (length: 104 in, height: 5 in)	2.521
Face	1,000 in ² of 0.5 in thick face	29.568

Chapter 3

Experimental Results

The research program described herein was carried out as series of several test sets whose results are presented separately, since each of them focused on particular aspect of the FRPH system being evaluated. To enhance the readability of this text, the goals of each test set, applied experimental techniques, experimental results and partial conclusions will be presented in individual sections devoted to each test set.

3.1 Series A

ASTM Standard C393-00 [ASTM 2000] requires that test specimens used to determine the flexural properties of sandwich panels should meet certain dimension restrictions. Specifically, the width of the specimen shall not be less than twice the total thickness and shall not be less than three times the dimension of a core cell. In the case of full-scale composite bridge deck members, these requirements can quickly lead to expensive test specimens with a wide cross-section. Justification of these parameters was an important concern to the researchers at the KSU prior to making general assumptions about the specimen size requirements for the rest of the experimental program. It was therefore decided to test five FRPH decks having the same face and core thickness and core depth, but varying width in order to evaluate the effect of width-to-depth ratio on the flexural properties. These specimens had nominal width-to-depth ratios between one and five, with the minimum nominal width of 6-in (150 mm) being equal to exactly three times the core cell lateral dimension of 2-in (50 mm).

Table 3.1: Series A - Dimensions and Description of Geometry

Property		A6	A12	A18	A24	A30
Total length	[in]	104.63	104.75	104.75	104.63	104.50
Core length	[in]	104.00	103.94	103.88	104.13	104.00
Total width	[in]	7.06	13.19	19.75	25.50	32.06
Core width	[in]	6.25	12.75	19.13	25.19	31.19
Total depth	[in]	5.94	5.94	5.94	5.94	5.94
Top face thickness	[in]	0.511	0.549	0.544	0.527	0.569
Bottom face thickness	[in]	0.496	0.512	0.528	0.510	0.591
Flats and flutes thickness	[in]	0.116	0.116	0.115	0.115	0.106
Number of flats		3	6	9	12	15
Number of flutes		3	6	9	12	15
Pattern - beginning		flat	flat	flat	flat	flat
		sin 90	sin 270	sin 270	sin 90	sin 270
		flat	flat	flat	flat	flat
		sin 270	sin 90	sin 90	sin 270	sin 90
	
Cells per length		26	26	26	26	26

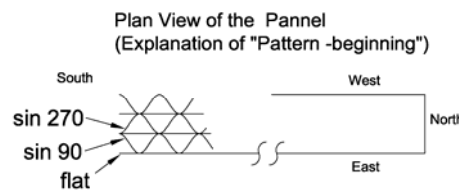


Table 3.2: Series A - Ultimate Load, Deflection, and Strain Data

Specimen	Ultimate Load [lb]	Ultimate Midspan Deflection [in]	Ultimate Bottom Midspan Strain [uE]
A6	20,954	2.48	9,072
A12	44,307	3.03	10,221
A18	48,878	2.49	N/A
A24	36,188	1.21	4,142
A30	100,806	2.61	8,500 (estimated)

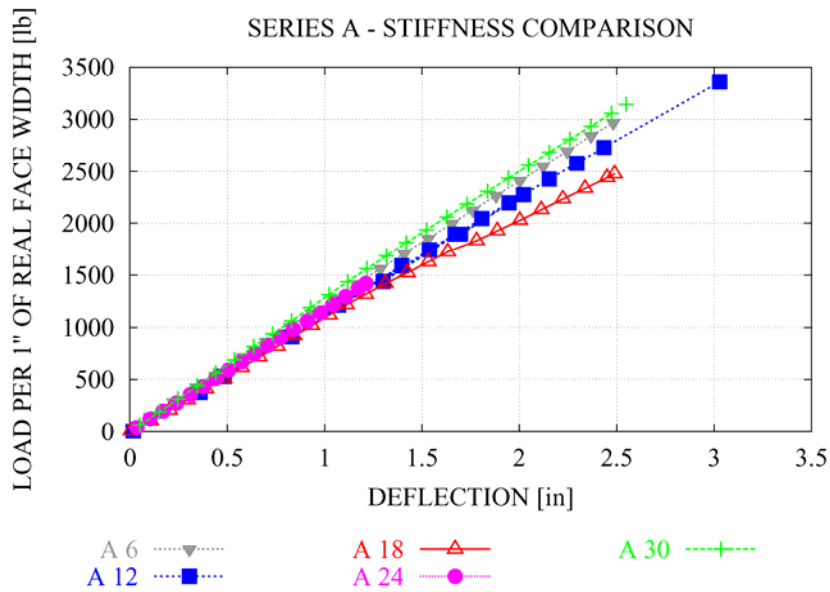


Figure 3.1: Stiffness Comparison of Specimens Tested in Series A

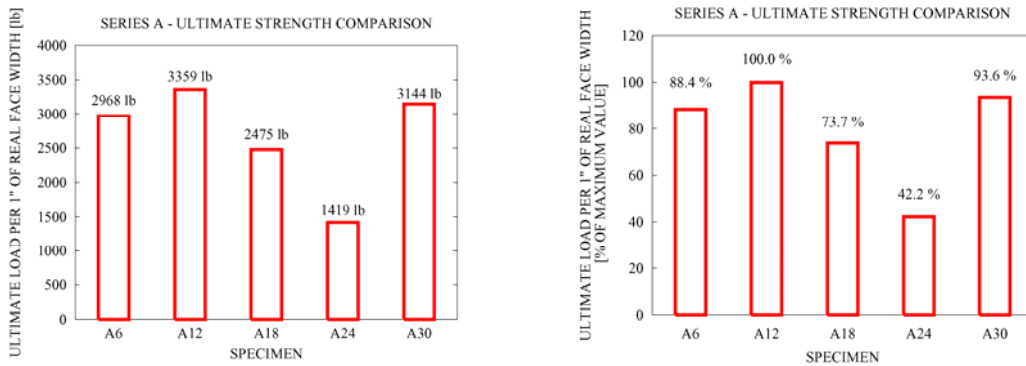


Figure 3.2: Comparison of Ultimate Load per Unit Width for Specimens of Series A

Table 3.1 lists dimensions of all specimens of Series A. Dimensions were measured at several places along the specimens and then averaged as shown in Table 3.1.

Figure 3.1 depicts the most important outcome of *Test Series A*, because crucial information can be deduced from it.

First, the stiffness per unit width is very consistent among all five specimens until a midspan deflection of about 1.2-in (30.5 mm) was reached, which corresponds to a span-to-deflection (L/d) ratio of 80. Taking into account the current design requirement of $L/d = 800$, we conclude that the stiffness is very consistent in the design load range. Also, all specimens behaved linearly up to the point at which their stiffness' began to diverge. Beyond this point, at higher load levels, small non-linearities (i.e. softening) were observed (especially for specimen *A18*).

Second, the ultimate strength values (per unit width) of the panels can be obtained from Figure 3.2 and Table 3.2. Compared to stiffness values, the ultimate strength per unit width embodies a significantly greater variance among the specimens of *Series A*. To understand this phenomenon, it is important to note that all decks were manufactured manually and that the failure mode of all specimens was a horizontal shear failure between the core and face panels. Quality due to the manual fabrication process would likely have the widest variation in the connection details of the panel, as the amount of resin, its proper distribution, and clamping force are all controlled by human decisions. Moreover, the resins generally have a greater variance in mechanical properties than do glass fibers. Since resin is the only means of transferring forces between the core and face laminates, and failure was always observed to initiate and propagate in these un-reinforced connection details, the greater variation in ultimate load carrying capacity is understandable.

Nonetheless, all of the specimens of *Series A* failed well beyond the design load level, which is almost always controlled by the live-load deflection limit ($L/d = 800$). This means that increasing the ultimate strength of these panels would not necessarily increase the design load, but definitely would increase the inherent safety of the structure. However, if a more consistent

flexural response was ensured, then perhaps the live-load deflection limit of $L/d=800$ could be justifiably reduced. The use of external wraps is one way to increase the ultimate strength of these members and reduce the level of variation noted for the un-reinforced core-face interface. This will be described in Sections 3.2 and 3.3.

After loading to flexural failure, the top and bottom faces of the specimens in *Series A* were removed to investigate the extent of damage to the core. While doing this, the flats and flutes were found to be completely undamaged. However, delamination between the flats and flutes was noted in the area below the spreader beam. This area of core delamination extended longitudinally, along the sides of the panel, to the ends of the panels.

3.2 Series A Repaired

All specimens of *Series A* (except for *A12*, which was cut into pieces for coupon testing) were rebuilt and then tested in flexure again. The repair was done by first removing the faces from the previously failed specimens. The faces were re-bonded back to their original position using three layers of 3-oz ChopSM placed between the core and faces to achieve a strong and resilient bond. Then wraps, composed of three layers of ChopSM, were applied over the edges of decks. The wraps were placed continuously over the most external flats. Each wrap was anchored 6-in (150 mm) deep on the surface of the faces (see Figure 3.3 for details). This repair method added extra material, resulting in a significant weight increase as listed in Table 3.3.

After failure, the faces were removed from specimens *A18* and *A24* in order to evaluate the damage to the core. Compared to the original specimens of *Series A* (where the flats and flutes were delaminated from each other under the loading area), the extent of core delamination in the repaired specimens was much smaller. However, some flats in the repaired beams were

ruptured (in tension) in the area below or close to the spreader beam. Reduction of the core delamination may be attributed to the wraps that served to confine the beam.

Tests on specimens of *Series A Repaired* are described in chronological order, because test results from earlier repaired panels influenced the instrumentation plan and loading of subsequent specimens.

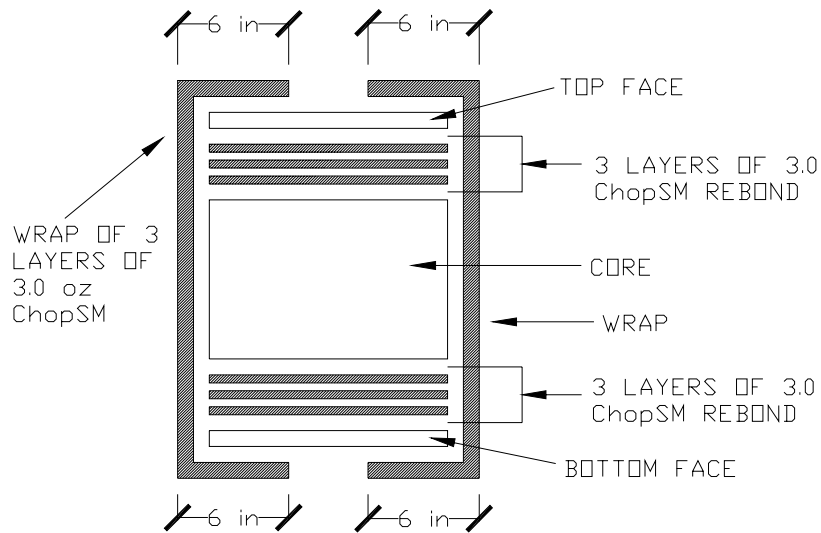


Figure 3.3: Schematic Drawing Showing the Re-bonding Layers and Wraps for the Repaired Specimens of Series A

Table 3.3: *Series A* - Comparison of Total Weight for the Original and Repaired Specimens

Specimen	Weight of original specimen [lb]	Weight of repaired specimen (with wrap) [lb]	Weight increase [%]
A6	67	105	57
A12	127	—	—
A18	191	299	57
A24	249	371	49
A30	312	453	45

— data not available, since specimen A12 was not repaired

3.2.1 A18 Repaired

For specimen *A18 Repaired*, strain gages were installed at the locations where the strain distribution (observed during the testing of specimens from *Series A*) was assumed to be altered by employing the external wraps. Three rosettes were mounted on the east side of the panel, while uniaxial gages were placed in longitudinal and transverse directions on the portions of the wrap that were anchored to the bottom and top faces (Refer to Figure 8.30 in Appendix B). Measured strains, however, did not indicate any significant change in the overall strain distribution when compared to specimens for the original *Series A*. This can be explained by considering following two facts: (1) the test was conducted in load-control mode which meant that, upon reaching the ultimate flexural capacity, failure was instantaneous. Therefore, any additional strains that might have occurred in the wrap immediately prior to the failure had only a very short duration and would not have been recorded at the regular data acquisition scanning rate used for the whole test. In other words, the load-control mode results in an explosive failure as soon as the total bond between the core and face laminates was destroyed. (2) The gages were mounted too far from the edges of the panel which reduced the opportunity to detect additional tensile strains being developed in the wrap. The gages should have been placed closer to the location where the wrap bridges the un-reinforced core-face interface instead of the location where the wrap is fully anchored to the face.

Specimen A18 Repaired failed by delamination of the wrap from the top face. Under the loading point, however, the spreader beam prevented the wrap from delamination by clamping it down and the wrap failed in tension instead (see photographs in Appendix B).

3.2.2 A24 Repaired

For this specimen, it was decided to further study the effect of employing wraps. Compared to specimen *A18 Repaired*⁷, gages were mounted as close to the edges as possible. Four groups of six gages were located on the top panel edges symmetrically about both longitudinal and transverse panel axes. In each group of three gages, two were gages perpendicular to the panel edge and were intended to measure tensile strains in the wrap and to possibly indicate stress concentrations closer to the edge. A third gage, parallel to the edge, was intended to pick up increased strain as the core-face interface was being delaminated, and the wrap consequently picking up more force. It was also decided to conduct the test in deflection-controlled closed-loop mode. This enabled the observation of a progressive failure.

Test results from specimen *A24 Repaired* confirmed that the wrap is indeed acting as a “clamp” to hold the panel together even after the resin (bond) at the core-face interface has failed. During loading, the initial failure of the panel (crushing at the support⁸ and core face delamination) occurred at a load of approximately 75 kips (333 kN) and was accompanied by a load “bang”. This noise was similar to that corresponding to other *Series A* specimen failures. When this occurred, however, the panel was still able to withstand considerable load, since the deflection was held constant. The remaining load on the panel was 63 kips (280 kN) (see graphs in Appendix B). The load drop was caused by a decrease in stiffness resulting from the core-face delamination. As expected, a small amount of horizontal movement had to occur to engage the wrap in tension. Yet, the wrap was able to keep the panel acting as a single structure due to the shear-friction phenomenon. Figure 3.4 shows the load vs. strain graph for 2 strain gages (G18,

⁷ Where gages were located on wrap about 3-in (76 mm) from the panel edge.

⁸ After the test, it was noted that hydrocal (used to provide uniform layer between bearing plate and the deck) was not distributed evenly. Especially, at the centerline of the beam, thicker layer of hydrocal was needed, because wraps increased total thickness of the panel close to the edges and created “depression” in between. This depression was not filled completely by hydrocal, which in turn resulted in higher stresses and crushing in the areas with full contact between the beam and bearing, see Figure 8.37 in Appendix B.

closer to the edge, and G19, below G18, further from the edge) mounted vertically on the wrap on the side of the panel. Until the maximum load 75 kips (333 kN) the tensile strain in the gages is essentially due to Poisson's ratio. Then, a sudden increase in strain from about 1,400 $\mu\epsilon$ to almost 3,000 $\mu\epsilon$ occurs as the load drops, indicating that the wrap is suddenly picking up increased tension. The specimen could sustain further loading in deflection control (from 1.614-in (41 mm) to 1.937-in (49 mm)), but never exceeded the previous peak load (see graphs in Appendix B). Ultimate flexural failure occurred when the wrap failed in bond and delaminated from the bottom face of the panel (see Appendix B).

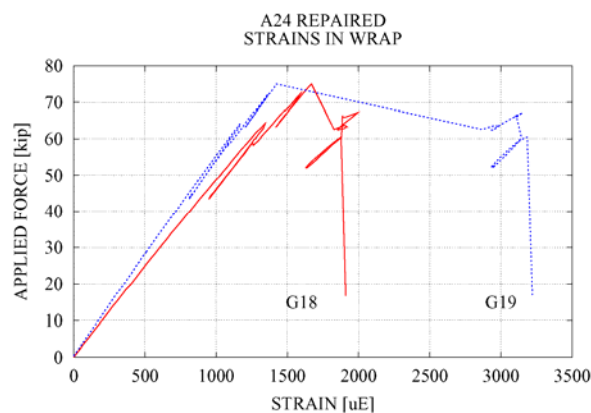


Figure 3.4: Development of Tension in the Wrap for A24 Repaired Specimen

Although the wrap in specimen *A24 Repaired* was able to prevent collapse of the panel after delamination at the core and face interface occurred, the specimen was not able to withstand the previous peak load. Therefore, if this specimen had been tested in load control, total failure would have immediately followed the initial horizontal shear failure.

It is worth noting that specimen *A24* failed at very low load when compared to other specimens of *Series A*, both before and after repair. Quality of the manufacturing process for this

specific specimen was thus questioned and the specimen was thoroughly visually inspected. Inspection after failure of the repaired specimen indicated that the core was not of uniform height, in other words it was not saw-cut to a uniform height during the manufacturing process. Therefore, imperfect bond between the core and face resulted at the locations of thinner core. Since the same core was used for both the original and repaired specimens, the ultimate load-carrying capacity was likely compromised in both cases and this specimen thus did not follow the typical trends of other Series A specimens.

3.2.3 A30 Repaired

Inspection of the *A30 Repaired* specimen prior to testing also revealed that this panel was poorly manufactured. Specifically, the bond between core and faces was observed to be essentially missing in certain locations at the ends of the panel⁹. The ultimate load for this panel¹⁰ was thus expected to be less than for an “ideal” specimen.

The panel was instrumented with 14 strain gages. Eight gages were mounted directly on the specimen to collect data for comparison with other specimens (e.g. maximum strain). The remaining six gages were mounted either to an aluminum strip (gages G1, G2, G5, G6) or to an aluminum rod (G3, G4) that were consequently glued or fastened to the panel to measure qualitatively the separation of faces from the core (refer to Figure 8.40).

About 10-in long aluminum strips were placed vertically on the side of the 6-in. deep panel, with the extra 2-in. of the strip on each end bent over the edges and glued to the bottom and top faces. The middle portion of the strip (6-in. long) remained unglued in order to measure a uniform tensile strain.

⁹ It was possible to slide a sheet of paper between the core and face.

¹⁰ For the acoustic emission load profile.

Aluminum rods with strain gages were inserted into a hole that had been drilled through the whole depth of the panel. The rods were “pre-tensioned” to 500 $\mu\epsilon$ by tightening the nuts that were securing the rods in the specimen. This was done in order to be able to sense also possible compression of the rod, that would result in a drop of the original 500 $\mu\epsilon$ strain.

Specimen *A30 Repaired* was loaded by manual deflection-control of the hydraulics to failure (see graphs in Appendix B). Similar to the test of *A24 Repaired* panel, the deflection-control resulted in the opportunity to observe residual strength after a global core-face delamination failure at a load of about 87 kips. The panel ultimately failed by wrap delamination (from the bottom face) along the North portion of the West side. Significant core-face separation was detected only by the strain gage mounted on the North aluminum rod. This is consistent with (a) the initial delamination that initiated at the North end of the beam and (b) the likelihood that corresponding core-face separation along the north edges was probably contained by the wrap on the edges. Therefore, no significant strain increase/separation was noted at these locations by strain gages on the aluminum strips. This also indicates that the “clamping effect” of the wrap diminishes towards the center of the panel due to the flexibility of the faces.

3.2.4 A6 Repaired

Among the specimens of *Series A Repaired*, Specimen *A6 Repaired* had the highest ratio of total wrap thickness (bridging the core-face interface) to the panel width. Therefore, it was anticipated that this panel could sustain a higher ultimate load per unit width than the other specimens of *Series A Repaired*, since a higher “clamping” force per unit width would be developed by the wrap. Furthermore, the *A6 Repaired* panel was completely encompassed by the wrap, which eliminated the failure mode of wrap delamination from the faces. In other words, fiber breakage was necessary prior to ultimate failure.

This specimen was instrumented with only eight strain gages, because the overall response was deemed to be the most important performance characteristic to study.

Visible and audible damage to the panel prior to the ultimate failure was insignificant. The panel failed by wrap rupture in tension below the loading point (see Figure 8.28 in Appendix B). It was also noted that the bottom face slid towards the center of the panel upon the failure (refer to Figure 8.29 in Appendix B). This is attributed to the fact that the interlocking material between bottom face and the core were sheared off and the horizontal movement was enabled – even without failing the wrap in tension – upon reaching critical force.

Specimen *A6 Repaired* had ultimate properties (ultimate load per unit width and ultimate shear flow per unit width) superior to that of all other panels tested.

Table 3.4: Series A Repaired—Ultimate Load, Deflection and Strain Data

Specimen	Ultimate Load [lb]	Ultimate Midspan Deflection [in]	Ultimate Bottom Midspan Strain [uE]
A6 Repaired	33,890	3.27	12,900
A18 Repaired	89,575	2.60	10,443 (extrapolated ¹)
A24 Repaired	72,260	1.61	6,187
A30 Repaired	86,956	1.58	6,737

¹ Strain gage went out of range, strain at ultimate load was extrapolated from load interval between 86,363 lb and 88,094 lb

3.3 32-ft-long Beams

Three 32-ft-long beams were analyzed in the scope of this project¹¹. Beams designated as *32-ft Damaged* and *32-ft Repaired* were tested at KSU while the *32-ft Clarkson* Beam was tested at Clarkson University. General information about the specimens’ geometry and test results is

¹¹ It is recommended to reader to refer to [Kalny et al. 2001], which includes evaluation of three 32-ft-long beams in great detail.

provided in Section 2.2 and Appendix B. In the following paragraphs primary focus is given to the beams that were tested at KSU.

3.3.1 Damaged Beam

The *Damaged Beam* specimen was fabricated by KSCI in August 2001. The specimen was 32-ft (9.75 m) long, 12-in (305 mm) wide and 31.5-in (800 mm deep). It represented a portion of a deck panel for a proposed bridge in New York. The specimen was designed to carry HS-25 highway loading [AASHTO 1996] and was shipped to Clarkson University (Potsdam, NY) for testing. Unfortunately, during the transportation process, the beam was damaged by a fork-lift operator in Pennsylvania. The damage consisted of partial delamination of the sandwich panel at the junction between the core and top face. The damaged area was approximately 10-ft (3.05 m) long. As an experiment, the *Damaged Beam* was shipped to KSU in September 2001 and loaded to failure in 4-point bending to determine the remaining stiffness and load carrying capacity. For this test, the face with the delamination was placed on the bottom (tension) side. The *Damaged Beam* failed at a total applied load of 40 kips (178 kN) by propagation of delamination from the south end of the original damage to the South end of the beam. On the north edge of original damaged interface some additional debonding occurred but did not extend to the supports. The beam stiffness remained nearly constant until failure.

3.3.2 Repair Procedure

After failure, the beam was returned to KSCI's production facility in Russell, Kansas, and repaired using only approximately 30 lb (14 kg) of new material. The repair was possible since the failure mode was a bond failure between the face (which had initial delamination) and core. Thus, the core and each individual face remained intact. In addition to rebonding the failed interface, a single additional layer of laminate was placed over the junction where the face meets

with the core. This was the first use of an external corner wrap in the test program. The wrap was intended to provide additional reinforcement across the previously delaminated joint and to perhaps increase the ultimate load-carrying capacity (this idea is similar to external shear reinforcing of concrete beams by FRP plates). In this particular case, the repair was done at the manufacturer's facility for cost-effectiveness (KSCI employees did not have to travel to KSU for the repair) and to maintain the test schedule. However, a similar repair process has already been performed by KSCI in the field. Since comparable quality control can be achieved in both the manufacturing facility and at bridge sites, the in-situ repair would be much preferred for a real bridge structure, as it would eliminate the cost of removal and transportation between the manufacturing facility and bridge site. Expenses for the repair were only a small fraction of the total cost required to manufacture a new member.

During the repair process, the beam was first inverted, so that the delaminated portion of the beam was on the top. The next step was to totally remove the face with the delaminated interface. Then, three re-bonding layers of 3.0 oz/ft² (915 g/m²) ChopSM were placed on the core. Next, vinyl-ester resin was applied to these re-bonding layers and distributed evenly using a painter's roller. Then, the removed face laminate was placed on top of the wet resin to restore its connection with the core. Finally, dead weight was placed on top of the face to produce a near-uniform pressure of roughly 75 psf (3.6 kN/m²) until the resin had cured. After removing the weight, an additional wrap layer of 3.0 oz/ft² (915 g/m²) ChopSM was placed over each of the four exposed face laminate and core joints. The location and properties of additional layers due to repair are provided in Appendix B. In addition, an external flat had been added to the core to enable application of the wrap layer. The undamaged *Clarkson Beam* also contained this additional flat laminate.

3.3.3 32-ft-long Repaired Beam

The *Repaired Beam* was sent to KSU for reloading to failure. It was tested with the identical set-up as the one used for the *Damaged Beam*. Similar to the test of *Damaged Beam*, the *Repaired Beam* was not loaded at a constant load rate to failure. Instead, the load profile was tailored for AE monitoring (see Figure 2.3). At a total load of approximately 97 kips (432 kN) the capacity of the load cells was approached so the test was paused and the load cells removed. Note, the similar beam at Clarkson University had failed at a total applied load of 75 kips (335 kN), so the researchers did not anticipate the previously damaged beam to exceed 100 kips (450 kN). Although direct measurements of load could not be obtained beyond this point, the value of applied load was extrapolated from corresponding readings of deflection and strain. The experiment had to be paused once more because the beam deflected beyond the range of the cylinders' stroke (see Appendix B). To resolve this problem, the beam was unloaded and wooden blocks were placed between the top face of the beam and cylinders. The beam was then re-loaded and failed at a total applied load of approximately 125 kips (560 kN). The failure was initiated by the debonding at the interface between the core and top face, exactly below the loading points, and was accompanied by core buckling. The initial separation propagated all the way to the North end of the beam. In the southern direction, however, the debonding propagated only about 3-ft (1 m) beyond the loading point. The interface between the bottom face and core was also ruptured, but damage to the bottom flange was limited to the vicinity of the loading points only.

As with the *Damaged Beam*, the *Repaired Beam* failed by rupturing at its weakest point, namely the resin bonding layer between the core and top face plate. This time however, the failure also caused the corner wrap laminates to fail (refer to photographs in Appendix B).

Between the loading points of the beam, the face laminates approached ultimate strain capacity (compare Table 2.3 with graphs in Appendix B).

3.3.4 Data Reduction Procedure

A nearly-linear response, typical for all-composite structures, was observed for both strains and deflections. The linear response might seem to be a little obscured when analyzing graphs in Section B.4. This is due to the fact that the procedure used to reduce huge measured data sets¹² involved extracting data points only for the “rising portions” of the load profile. Moreover, only the “rising portions” of the load profile with current maximum value for load were considered. To illustrate how the data set was reduced, consider following example: To extract 20 points along the load vs. deflection graph for “increasing load only”, the maximum achieved load F_{\max} is divided into 20 equal intervals:

$$\left\langle 0, \frac{F_{\max}}{20} \right\rangle, \left\langle \frac{F_{\max}}{20}, \frac{2F_{\max}}{20} \right\rangle, \dots, \left\langle \frac{19F_{\max}}{20}, F_{\max} \right\rangle$$

C++ code was developed to perform the data reduction. The original (unreduced) data file was then used as the input file for the program. At the beginning, all of the 20 intervals, described above, are marked as “unused”. Input file was then scanned line by line (each line contained measurements from all of the sensors used in the test) and if load value fell within the “unused” interval, then the interval was marked “used” and the corresponding line from the original data file saved to the reduced data file. Using this algorithm, a reduced data file was created and includes evenly spaced data points for the first occurrence of the load at desired load level—note that loading, unloading and reloading is typically used in the loading profile to accommodate the AE monitoring.

¹² Loads, deflections, and strains were captured for more than 10,000 points during the 32-ft-long *Repaired Beam* test

This data reduction method helps to explain why there is a sudden change in the trend of measured strains, especially for the rosettes, at loads of about 100 kips (445 kN) and 120 kips (534 kN). Before exceeding the previously indicated two load levels (in the first case to remove the load cells and in the second case to insert the wooden blocks between the specimen and cylinders), the specimen was unloaded from the maximum load. Then the specimen was reloaded past 100 kips (445 kN) and 120 kips (534 kN). There was probably a change in structural integrity that initiated during the previous loading but was detected only after unloading to zero load and subsequently reloading. Because the data reduction method for the “increasing load only” case, as described earlier, was used to reduce the data set, the change in structural behavior integrity is seen as a sudden change in the load-deflection graph when the load increases above the previous peak values during reloading. In other words, if only the data from the reloading limbs are extracted and plotted, then a linear response is observed.

Test results from the *Repaired Beam* demonstrated that delamination damage to FRPH panels can be adequately repaired.

3.3.5 Comparison of Test Results from 32-ft-long Specimens

The *Repaired Beam* was able to carry more load than a similar undamaged specimen that was tested in 4-point bending at Clarkson University. The *Clarkson Beam* failed by horizontal shear at a total applied load of 75 kips (335 kN). The significant increase in the ultimate load-carrying capacity for the *Repaired Beam* may be attributed to the wrapping layer that was applied to the *Repaired Beam* (as a part of repair process) but not to the *Clarkson Beam*. The wrap contribution is analyzed in depth in Chapter 4.

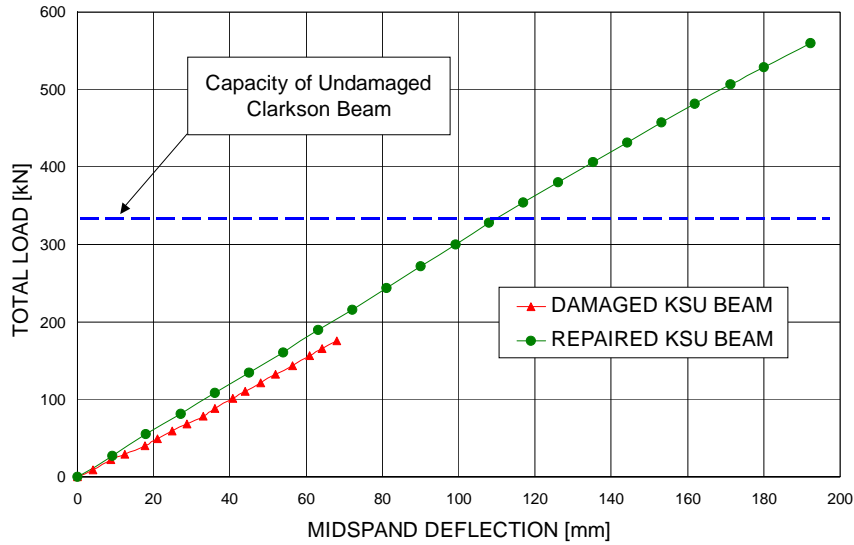


**Figure 3.5: Total Load vs. Deflection
(Comparison of Damaged, Repaired and Clarkson 32-ft-long Beams)**

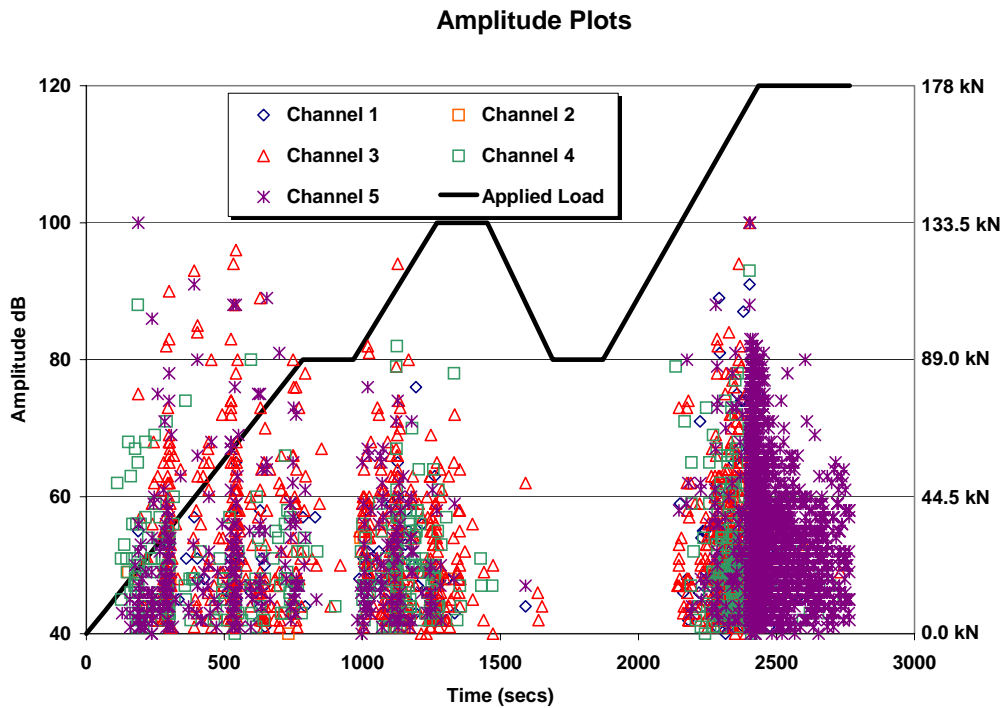


**Figure 3.6: AE Results for Damaged Beam - Amplitude vs. Time
(Graph Provided by G. Ramirez, University of Kansas)**

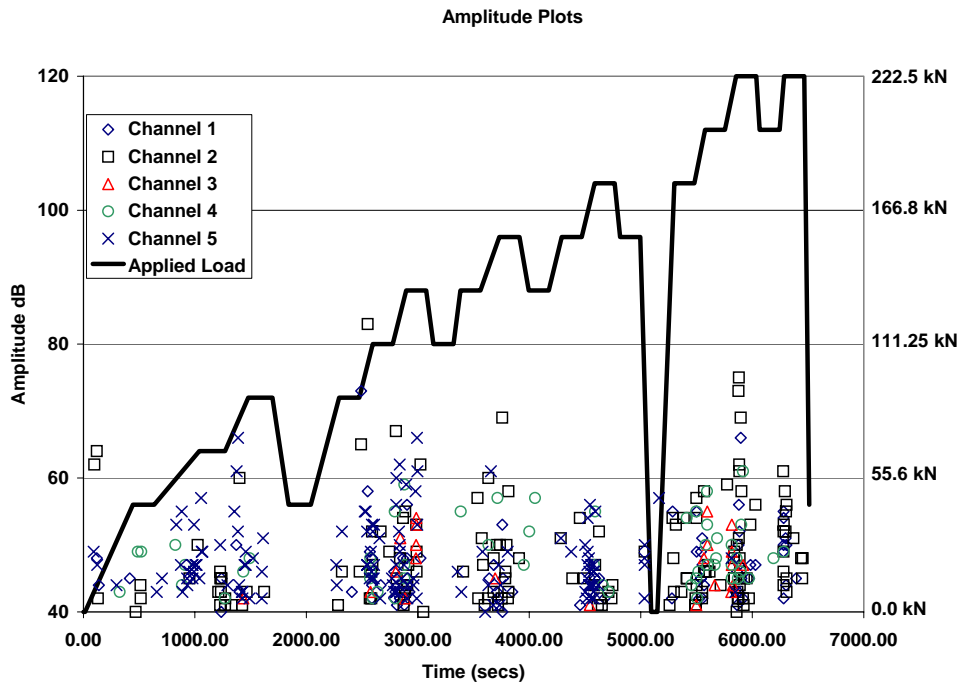


Figure 3.7: AE Results for Repaired Beam - Amplitude vs. Time (Graph Provided by G. Ramirez, University of Kansas)

Figure 3.5 shows that the *Repaired Beam* was a little stiffer than the *Damaged Beam*. This is reasonable, since the *Repaired Beam* contained one extra flat plus the rebonding layer. Ultimate loads for the three beams are also apparent from Figure 3.5.

AE data was also collected and compared to the two 32-ft-long beams tested at KSU. Information about AE monitoring, including two graphs (Figures 3.6 and 3.7), were obtained from Dr. Ramirez, KU. For the *Damaged Beam*, AE records (Figure 3.6) show an almost immediate activity with applied load. High amplitude hits at the beginning of emissions are indicative of a large particle movement usually associated with damage growth or high levels of mechanical rubbing. From Figure 3.7 it is notable that emissions of the *Repaired Specimen* were considerably lower than those recorded for the *Damaged Beam*. This indicated that the repair

procedure had been successful in bringing the Repaired Beam to a level superior to that seen on the first test.

3.4 Panels Manufactured with Internal Steel Reinforcement

Two panels with embedded steel rebar in the face laminates and corner wraps were tested. One of the panels contained two 13-mm (#4) bars in the bottom face, while the other panel had two 13-mm (#4) bars in both top and bottom faces. KSCI fabricated these panels in order to investigate the possibility of increasing stiffness of the panels by reinforcing them with steel. Steel is significantly stiffer than the laminate of top and bottom faces (compare $E_{steel} = 30 \text{ Msi}$ to $E_{faces, 0 \text{ deg}} = 2.796 \text{ Msi}$), but the total steel volume in the panel is limited by its high density. Higher percentages of steel in the panels would result in a considerable weight increase and would thus reduce the light-weight feature of the panels.

Both a simple model (based on the properties of a transformed section) and test results indicated that embedding small amount of steel in the panel does not significantly alter the behavior of the panels. The testing, however, provided valuable experimental data that extended the database of test results for sandwich panels. As expected, the panel with four rebars could sustain slightly more load and was a little stiffer than the panel with only two embedded rebars. Both panels failed by tension of the wrap, as shown in Appendix B.

3.5 Double-Shear Specimens

Double-Shear sandwich panel specimens were also fabricated by KSCI and tested at KSU as part of this research program. The objectives of these tests were to directly assess the shear capacity of the core-face interface, to demonstrate the wrap effectiveness on two sets of identical unwrapped and wrapped specimens¹³, and to experimentally determine the friction coefficient, μ , between

¹³ Note that for specimens of *Series A* and *32-ft-long Beams*, wrapped specimens were also repaired specimens which resulted in addition of extra rebonding layers and stiffness increase.

the core and faces that could be used for shear-friction design. These *Double-Shear* specimens were manufactured by KSCI according to the general specifications provided by KSU.

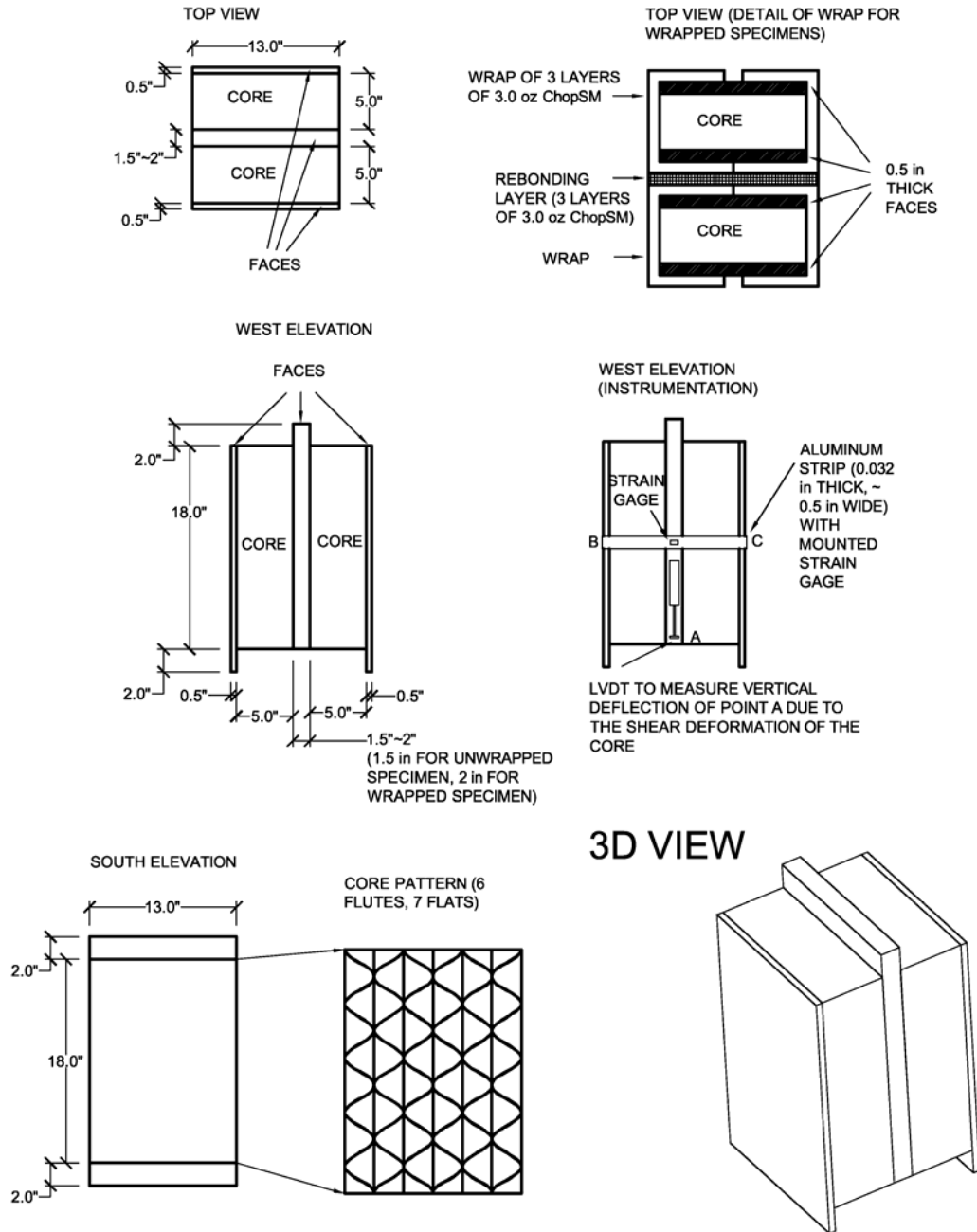


Figure 3.8: Double Shear Specimen

Each *Double-Shear* specimen was essentially composed of two smaller FRPH panels [each 18-in (450 mm) long, 13-in (330 mm) wide and 6-in (150 mm) deep] “glued” on top of each other. The two most external faces extended over the core about 2-in (50 mm) in one longitudinal direction, while the two internal (glued together) faces extended the same distance in opposite longitudinal direction (see Figure 3.8). The face extensions in longitudinal direction were used to provide contact loading area and to accommodate shear deformation.

Nine *Double-Shear* specimens were manufactured. Six of them, designated *A1* to *A6*, did not incorporate wraps while the three remaining specimens (*C1* to *C3*) were wrapped. Prior to testing, steel plates were mounted to the extended faces using hydrocal. The top plate had a double-T shaped cross-section of double-tee, while the two bottom plates were flat steel plates. These plates were used to level the specimens (since they were not manufactured with perfect dimensions), so that the vertical applied load could be applied nearly-uniform to the center face. In addition to the plates, a small I-Beam was placed on the top plate to ensure proper load distribution from the head of loading machine.

The original test plan was to conduct tests on the “unconfined” specimens *A1*, *A2*, *A3*, *C1*, *C2* and *C3* first. Specimens would be placed in the testing machine and the load would be statically applied to the I-Beam until failure occurred. Specimens for the “unconfined” test would be instrumented with two LVDTs to measure shear deformation of the core and two aluminum strips with strain gages to determine relative deformations between the external most faces (see Figure 3.8 for specimen dimensions and instrumentation).

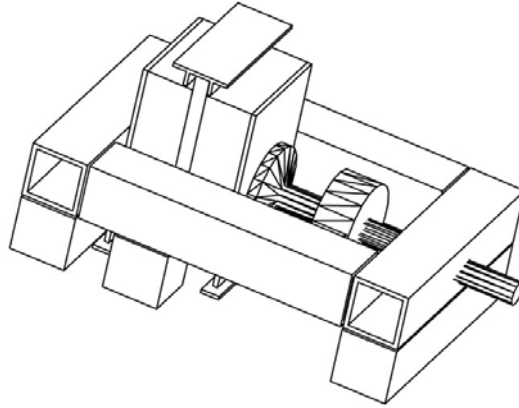


Figure 3.9: Double Shear Specimen - Test Setup For “Confined Test” (2-in Thick Steel Plates Would Be Placed Along the External Faces to Ensure Proper Transfer of Lateral Force to the Load Cell)

During the second test, specimens *A4*, *A5* and *A6* would be placed inside steel frame with a load cell (Figure 3.9) to measure the lateral force that is being developed by face core separation prior to ultimate shear failure. The steel frame was designed to be very stiff relative to the panels in order to confine the specimens and to measure the maximum lateral force. Under the anticipated maximum load of 50 kips, the longitudinal extension of the steel frame was designed to be only 0.005-in. The original plan was however changed as a result of the findings during the first few tests. These changes are explained in the following paragraphs.

The following sections list the findings from the double-shear tests in chronological order, as well as key observations and modifications to the test setups. These subtle changes in the test setups incorporated the results of numerous discussions about how to achieve a pure shear failure and how to best test the “imperfect” specimens that prematurely fail along the glue-line between adjacent panels. Suggestions for a new design of the shear specimens are also included.

3.5.1 Results from Tests of Unconfined Unwrapped Double-Shear Specimens (A1, A2, and A3)

A1 was the first specimen tested. During the loading of A1, a sudden increase of strain in the aluminum strip (from essentially 0 $\mu\epsilon$ to about 1; 300 $\mu\epsilon$) occurred. This was associated with splitting of the specimen along the glue line between the two halves (see Figure 3.10).

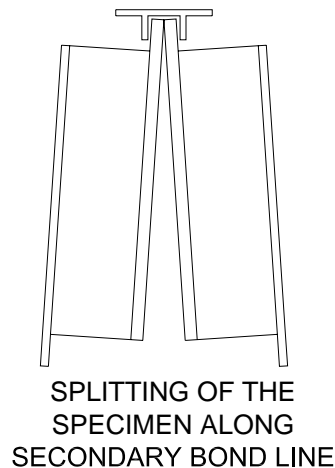


Figure 3.10: Splitting of the Double-Shear Specimen

It was also noted that the bottom opening was growing with increasing load. Upon reaching a load of 40 kips, the specimen was unloaded so that nylon straps could be loosely placed around the specimen for protection in case of a sudden failure. Upon reloading, the test was terminated prior to reaching the previously attained load of 40 kips, because the specimen splitting was so extensive that the validity of the data as data for “pure shear” was questionable.

Premature failure occurred along the line where the two panels composing the specimen were bonded together. To prevent this undesired failure, it was decided that future specimens should have an interior face that was laminated all at once. It was, however, believed that the

splitting can be prevented by introducing either external (frame around the bottom of the specimen) or internal (C-Clamps that would clamp the internal faces together at the bottom of the specimen, i.e. at the point where the splitting is initiated) restraints.

A3 specimen was tested the same day as *A1* specimen and because no C-Clamps or steel frame were available, wood was placed between the bottom of the specimen and the frame of the testing machine to prevent the splitting described earlier:

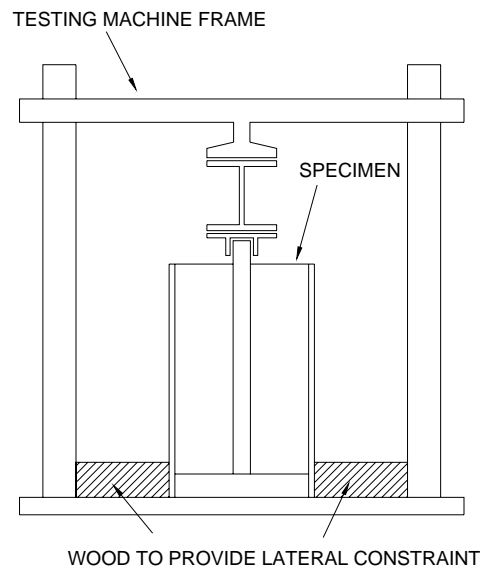
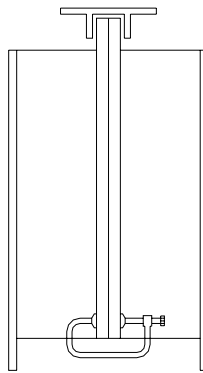


Figure 3.11: Lateral Constraint for Double-Shear Specimen A3

Placing the external constraints (wood in this case) around the specimen had two effects. (a) The desired effect was that splitting along the secondarily bonded interface was prevented. (b) The undesired effect was that the whole specimen was somewhat clamped and the shear friction, as described in Chapter 4, could have taken place. This was an unwanted effect for the unwrapped specimens. Thus, under this loading condition, the effect of shear friction due to the wrap (for the wrapped specimens) could not be directly compared to unwrapped specimens

(because shear-friction was likely introduced due to the external restraints). It was therefore decided to use C-Clamps to clamp the internal faces together for the remaining tests.

A1 (Re-instrumented, C-Clamped) was the same specimen that was previously loaded to 40 kips. The LVDT brackets and aluminum strips were re-mounted on the specimen since they separated during the previous test. The split interface was not re-glued, it was held together by the double-tee shaped steel member at the top and C-Clamps at the bottom (these were also used to prevent splitting, refer to Figure 3.12), as discussed earlier.



SIX C-CLAMPS WERE USED TO RESTRAIN THE BOTTOM PART OF THE SPECIMEN FROM SPLITTING

Figure 3.12: C-Clamps on Re-Instrumented Double-Shear Specimen A1

During the loading, it was noted that the specimen started to separate again in the middle of the specimen. Nonetheless, it was held together at the top (double-tee steel plate) and bottom (C-Clamps). Specimen *A1* was loaded until failure and failed in shear between core and face.

The test setup for double-shear specimen *A2* was identical to *A1 (Re-instrumented, C-Clamped)*. Although the specimen had not previously failed along the secondarily bonded interface, this interface separated in the middle of the specimen so that it was possible to “see

through the specimen.” Specimen A2 failed in shear between the core and face. The fact that the secondarily bonded interface split in the middle indicates that there was still tension being developed between the two halves of the shear specimen, even though it was held together at the top and bottom (refer to Figure 3.13).

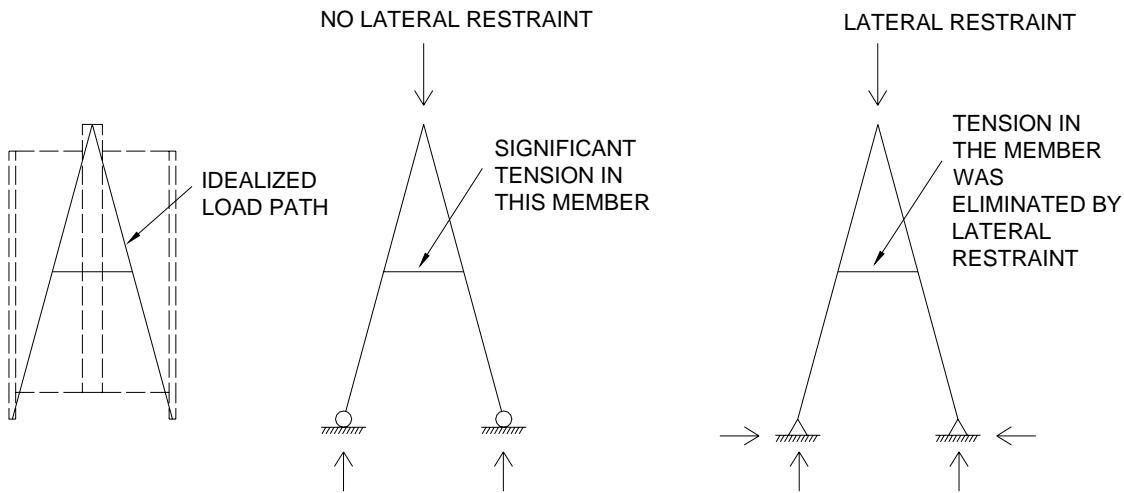


Figure 3.13: Impact of Lateral Constraint on Double-Shear Specimens

Therefore the failures for A1 (*Re-instrumented, C-Clamped*) and A2 specimens were due to the combination of shear and tension. By introducing the external frame to provide lateral constraint, the tension can be eliminated. However, when doing this, the undesired clamping for the unwrapped specimens (mentioned earlier) is reintroduced.

As a result of the observations from specimens A1 and A2, the researchers decided to use external lateral constraint in the form of a “low-profile” steel frame. The gap between specimen and “low-profile” frame was then filled by hydrocal (see Figure 3.14). By keeping the frame as “shallow” as possible and by placing it around the very bottom of the specimen (below the level of the core), the clamping effect would be greatly reduced.

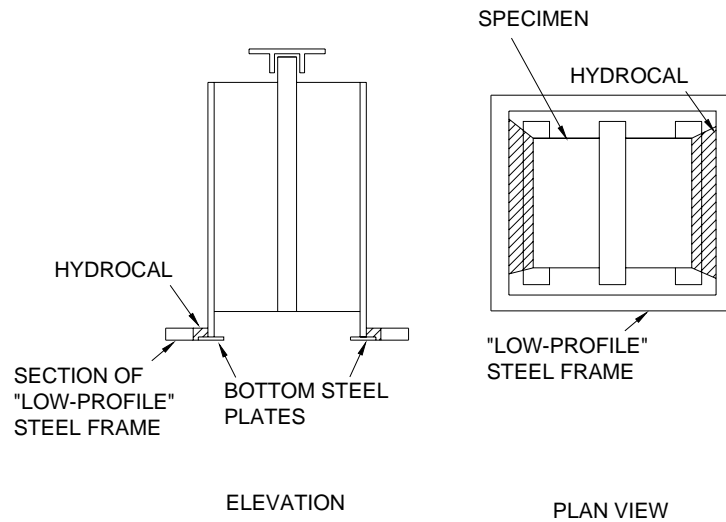


Figure 3.14: Lateral Restraint of Double-Shear Specimens by a Steel Frame

3.5.2 Results from Tests of Unconfined Wrapped Double-Shear Specimens (C1, C2, and C3)

Wrapped specimens C1, C2 and C3 were tested with both C-Clamps and a low-profile steel frame.

C1 was the first specimen tested with both C-Clamps and the low-profile steel frame around it. This specimen did not split in the middle. For higher loads, the specimen expanded laterally due to Poisson’s effect and the “feet” (bottom face extensions), being restrained from outward lateral deformation by the low-profile steel frame, tilted inward.

C2 was the specimen obtaining the highest ultimate load. Loading was stopped when all of the C-Clamps broke. Prior to ultimate failure, progressive delamination of wraps from the faces was observed (on the outer faces white (delaminated) areas were forming upwards from the bottom of the specimen).

C3 failed in the similar fashion as specimen *C1*.

3.5.3 Results from Tests of Confined Unwrapped Double-Shear Specimens (A4, A5, and A6)

The purpose of this test series was to determine the magnitude of lateral force being generated when the specimen is restrained from lateral movement and vertical forces on the core-face are transferred by shear friction after bond failure.

Stiff steel frame was manufactured and placed into the testing machine (refer to Figure 3.15). To ensure proper alignment, bottom and top steel plates were mounted on each specimen using hydrocal. Specimen was then placed inside the steel frame (Figure 3.15) and surrounded by two 2-in thick steel plates for proper transfer of lateral force into the load cell. The steel plates were shimmed with wooden blocks in order to closely adhere to the specimen above the bottom plates (Figure 3.18). The last step was to place the load cell inside the steel frame (Figure 3.17). Threaded rod was inserted inside the hole drilled through the channel section of the steel frame. The load cell was then screwed onto the inside end of the threaded rod. Nut placed on the threaded rod inside the frame was tightened to develop compression force of about 300 lbs. Spreader beam with welded brackets for LVDTs was placed on the top double-tee steel plate (Figure 3.16).

Specimens were loaded by manual deflection-control of the hydraulics—desired load rate was 3000 lbs/min, but did vary slightly according to the skills of an operator.

The lateral force was almost constant until point closely preceding the first peak load (refer to graphs in Appendix B), which is likely associated with bond line glue failure. First peak load was followed by an abrupt drop in applied vertical load as well as a steep increase in lateral force. From this point on, most of the shear force was likely carried by shear friction between the core and faces. Second peak in vertical load corresponded to reaching critical level of shear flow

on the core-face interface that could not have been transferred by frictional forces. The ratio of lateral force to applied vertical load at this point corresponds to the coefficient of friction, μ , of the core-face interface. This μ is however valid for “almost perfect confinement,” because the steel frame surrounding the specimen was designed to be extremely stiff. The μ for more flexible wrap confinement would have lower values because the softer wrap enables some separation.

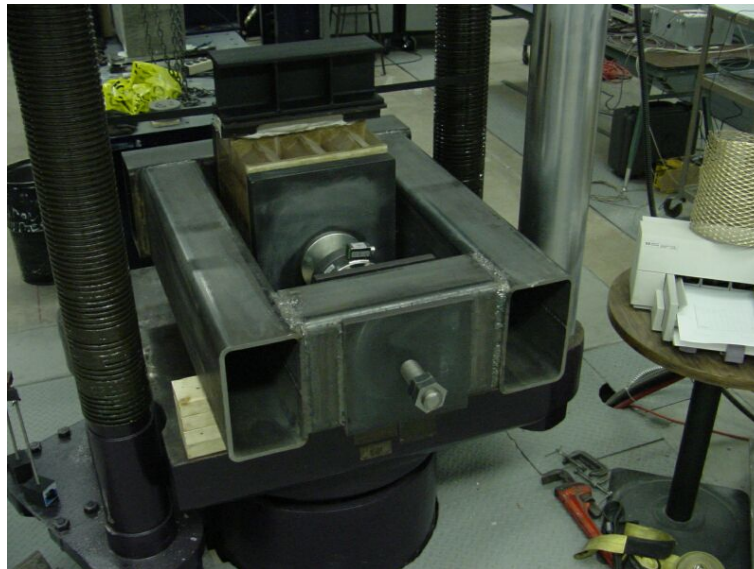


Figure 3.15: Overall View of Confined Double-Shear Specimen, Steel Plates and Confining Steel Frame

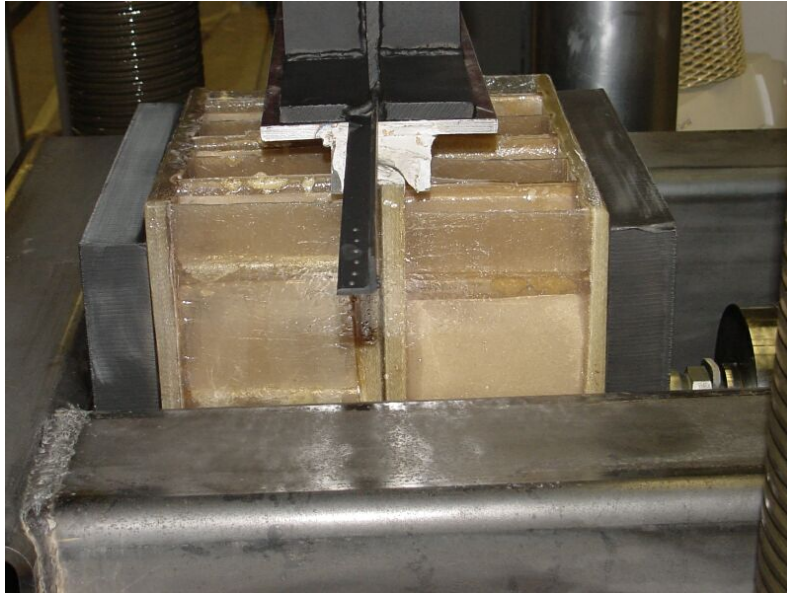


Figure 3.16: Detail of the Spreader Beam, Steel Plates and Top Portion of Confined Double-Shear Specimen

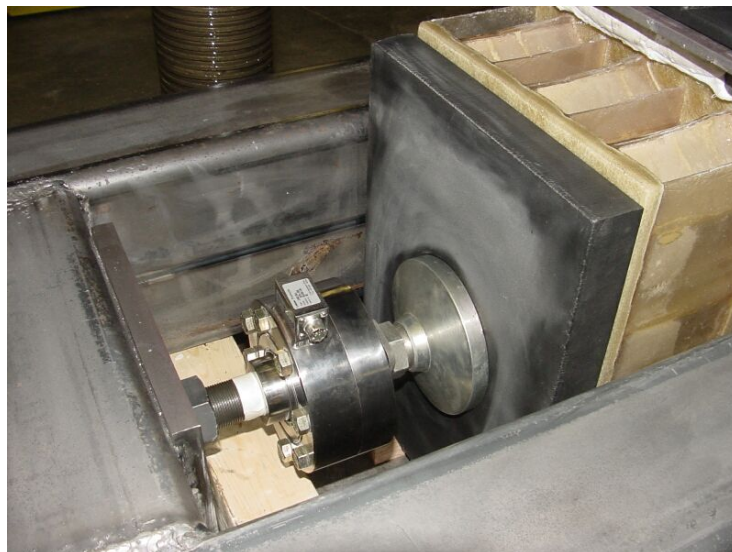


Figure 3.17: Load Cell to Measure Lateral Force Developed by Confined Double-Shear Specimen



Figure 3.18: Detail of the Bottom Portion of Confined Double-Shear Specimen, Steel Plates are Supported on Wooden Blocks (Photo)

3.5.4 Summary of Test Results for Double-Shear Specimens

Table 3.5 lists ultimate applied load and ultimate shear flow for all tested *Double-Shear* specimens. It is notable that both confinement and external wraps resulted in higher ultimate loads when compared to unconfined unwrapped specimens. The wraps increased ultimate shear capacity slightly more than confinement, as can be seen from Table 3.5. Graphs of load vs. deflections and load vs. strains are available in Appendix B¹⁴.

¹⁴ It is important to bear in mind that some data are not plotted to the ultimate load. This is because the strain data after the aluminum strip ruptured or deflection data after the LVDT bracket separated from the specimen are meaningless.

Table 3.5: Double-Shear Test—Results

Specimen	Ultimate Load [lb]	Ultimate Shear Flow per Corrugation Unit [lb/in]
A1	50,900	236
A2	67,300	312
A3	77,700	360
C1	86,200	399
C2	103,000	477
C3	78,700	364
A4	80,600	373
A5	85,400	395
A6	77,300	358

NOTE:

- A1, A2, A3 ... unconfined, no wrap
- C1, C2, C3 ... unconfined, with wrap
- A4, A5, A6 ... confined, no wrap

The ultimate shear flow per corrugation unit was determined as:

$$\frac{(Ultimate\ Load)/2}{(18\ in)(6\ corrugation\ units)}$$

Comparing Table 3.5 with Figure 4.6 indicates that higher ultimate shear flow was achieved for some flexural panels than for *Double-Shear* specimens. This is unexpected especially for confined *Double-Shear* specimens (A4, A5 and A6), because no such confinement exists in flexural test panels. In addition, resin bond line in flexural specimens is strained by combination of stresses, while failures of *Double-Shear* specimens are dominated by shearing stresses.

Testing of confined *Double-Shear* specimens confirmed occurrence of shear friction and provided some estimate for friction coefficient, μ , as a ratio of lateral force and applied vertical

load. However, a reliable determination of ultimate shear flow—based on resin bond line failure or shear friction phenomenon—has not been attained.

Based on research conducted in the scope of this project, the ultimate horizontal shear capacity of KSCI's panels can be determined from Table 3.5 and Figure 4.6. The design should be based on this experimentally-determined ultimate horizontal shear capacity. Designer should take into account the effect of section depth on the ultimate shear flow. As the design of KSCI's panels is always deflection controlled, more reliable criteria for ultimate capacity will increase the factor of safety, not the load that can be placed on the structure. The lowest factor of safety, calculated as the ratio of ultimate load and service load, was 11 (for *32-ft-long Clarkson Beam*, not taking into account *32-ft-long Damaged Beam* with pre-existing damage).

3.6 Fatigue

Four specimens of almost identical dimensions and geometry (refer to Appendix B for details) were cut from a large panel for the evaluation of fatigue performance. Each panel was approximately 8-in (200 mm) deep, 20-in (500 mm) wide, and 14-ft-and-5-in (4.4 m) long. The first specimen (*Fatigue Baseline*) was tested under static load to failure to determine the base strength and stiffness, and to select load levels for fatigue testing of the remaining specimens. Two of the remaining specimens (*Fatigue Specimen 1*, *Fatigue Specimen 3*) were tested under cyclic loading conditions. *Fatigue Specimen 1* was subjected to 11,000,000 *cycles* of load levels producing a span-to-deflection ratio of 400, while *Fatigue Specimen 3* was subjected to 5,000,000 *cycles* of load levels inducing a span-to-deflection ratio of 200. Both fatigue specimens performed extremely well, as failure under cyclic loading did not occur, loss of stiffness was insignificant, and increase in initial deflection (due to creep) was relatively small. The following sections provide detailed information about the two fatigue tests.

3.6.1 Fatigue Specimen 1

Fatigue Specimen 1 was instrumented with two strain gages and two LVDTs, each located at the mid-span of the specimen. This specimen was loaded in 4-point bending. The applied load ranged from a minimum of 500 lb (2,220 N) to a maximum of 5,400 lb (24,020 N). The maximum load was chosen to be equal twice the design load, i.e. this load resulted in a span-to-deflection ratio (L/d) equal to 400. The applied load had a sinusoidal profile and was applied with frequency of 3.25 Hz. The test was targeted for 10,000,000 cycles, or until failure occurred.

According to the initial test plan, the researches proposed to pause the cyclic loading every 250,000 cycles¹⁵ and conduct a static test. Each static test consisted of loading the specimen from 0 lb (0 N) to 5,400 lb (24,020 N), and then unloading it back to 0 lb (0 N). During the static test, values of load, deflection, and strain were recorded. Cyclic loading was initiated immediately after each static test, so the only time period when the specimen was at rest was between end of the cyclic loading and the beginning of the static test. Early during the test, however, it was observed that the specimen was not experiencing any apparent change in stiffness and the test plan was therefore slightly altered. Tests were then run over the weekends to accumulate as much as 750,000 cycles between two consecutive static tests. Also, the specimen was subjected to additional 1,000,000 cycles of loading, since the lab equipment was not immediately needed for other tests after the 10,000,000 cycles had been achieved.

Figure 3.19 shows what could be called the “static tests timeline.” This graph is particularly important when discussing other plots and should be referred to when addressing time dependent behavior. From Figure 3.19, it can be seen that the static test after 3,000,000

¹⁵ For given frequency this number corresponds to a little less than 24 hours of cyclic testing.

cycles was taken after almost three weeks of down time due to a temporary lab shut-down, and this fact in turn resulted in a “recovering” of some previously accumulated creep deflection.

Figure 3.20 shows that the specimen did experience some creep deformation during cyclic loading. With rising number of load cycles placed on the specimen, the initial deflection before each static test exhibits a rising trend. The exception is after 3,000,000 cycles, when the initial deflection decreased by 0.015-in (0.4 mm). This was likely due to the fact that the specimen was unloaded for nearly three weeks between end of cyclic loading and the beginning of the next static test. This unloaded period would have allowed some of the recoverable creep deflection to diminish. Between 8,000,000 and 11,000,000 cycles the rising trend of initial deflections is less pronounced.

While a small change in the initial deflection (likely due to creep) was detected for *Fatigue Specimen 1*, there was essentially no softening of the structure during the 11,000,000 cycles of load. This can be concluded from the graphs of load vs. midspan deflection and load vs. strain (Figures 3.21 and 3.22) recorded during static tests that were conducted throughout the cyclic loading.

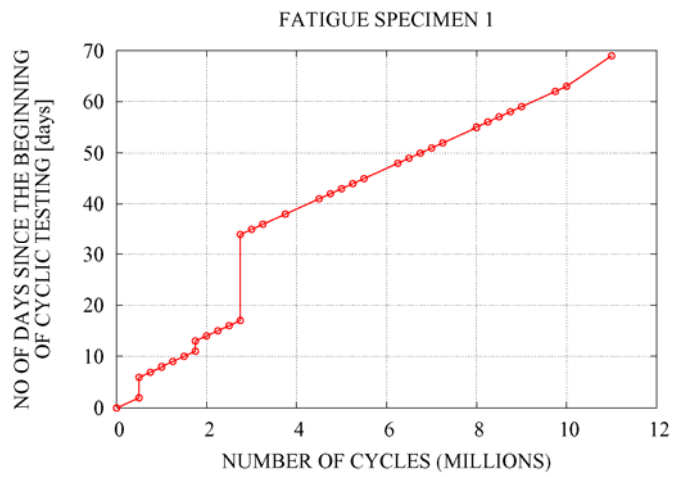


Figure 3.19: Number of Days Between Beginning of the Test and Each Static Reading vs. Number of Accumulated Cycles (Fatigue Specimen 1)

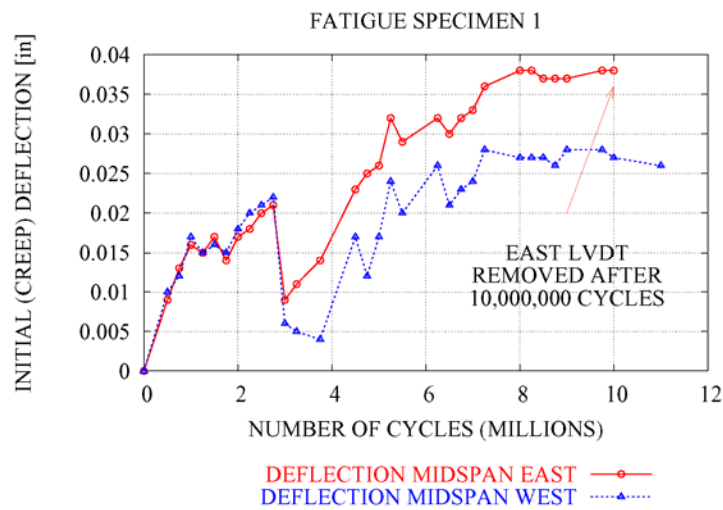


Figure 3.20: Initial (Creep) Deflection on the Beam Prior to Each Static Test vs. No. of Applied Cycles (Fatigue Specimen 1)

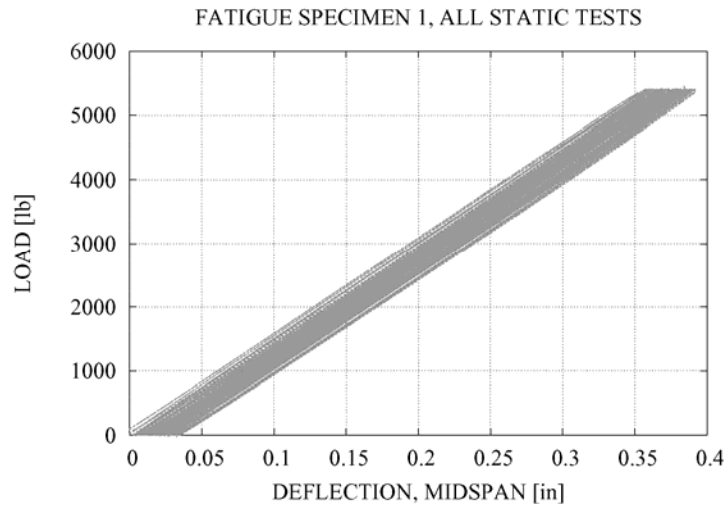


Figure 3.21: Load vs. Deflection for All Static Loadings (Fatigue Specimen 1)

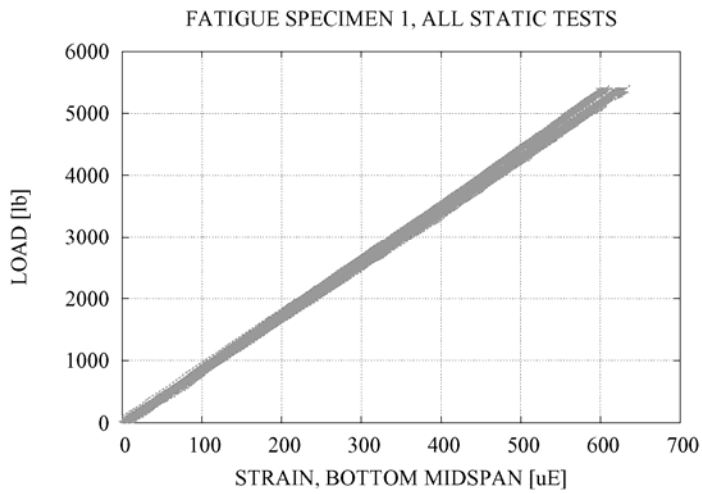


Figure 3.22: Load vs. Strain for All Static Loadings (Fatigue Specimen 1)

3.6.2 Fatigue Specimen 3

Fatigue Specimen 3 was tested after *Fatigue Specimen 1*. The test setup for this specimen was also 4-point bending, with an applied load range of 500 lb (2,250 N) to a maximum of 10,775 lb (47,930 N). The maximum load was selected to create a span-to-deflection (L/D) ratio of 200, or four times the design load, since these panels are typically deflection controlled. This corresponded to a maximum midspan deflection of 0.72-in (18 mm) in the 12-ft (3.65 m) span. The sinusoidal load profile was applied at a frequency of 1.0288 Hz. The test frequency was limited by the load system capabilities.

Behavior of *Fatigue Specimen 3* was very similar to that of *Fatigue Specimen 1*. A change in stiffness with increasing number of applied cycles was not observed. In fact, the stiffness based on both strain and deflection measurements were essentially constant with only random fluctuations. The initial (creep) deflection was about twice the value for *Fatigue Specimen 1*. This is reasonable since the maximum load for *Fatigue Specimen 3* was twice the maximum load for the first fatigue test.

Between 3 and 5 millions cycles, the hydraulic loading system experienced several shutdowns as a result of exceeding preset error limits in the test controller. These resulted in extended periods of rest for the deck between two static tests. This is the probable reason for the “recoverable” creep deflection noted during this period (refer to Figure 3.24).

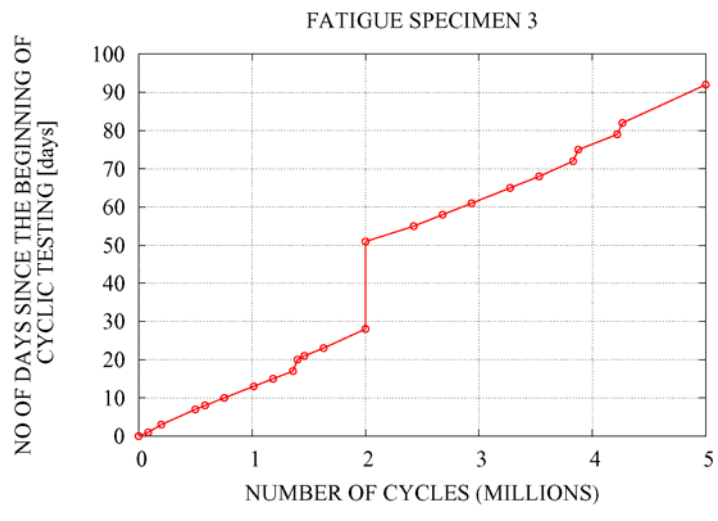


Figure 3.23: Number of Days Between Beginning of the Test and Each Static Reading vs. Number of Accumulated Cycles (Fatigue Specimen 3)

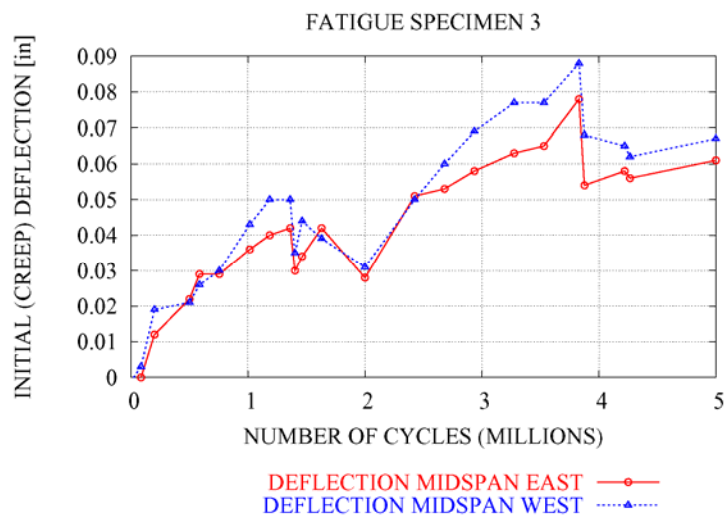


Figure 3.24: Initial (Creep) Deflection on the Beam Prior to Each Static Test vs. No. of Applied Cycles (Fatigue Specimen 3)